NASA TN D-984

TECHNICAL NOTE

D-984

AERODYNAMIC EFFECTS OF SOME CONFIGURATION VARIABLES ON THE AEROELASTIC CHARACTERISTICS OF LIFTING SURFACES AT MACH NUMBERS FROM 0.7 TO 6.86

By Perry W. Hanson

Langley Research Center
Langley Air Force Base, Va.

NATIONAL AERONAUTICS AND SPACE ADMINISTRATION
WASHINGTON

November 1961

1A

NATIONAL AERONAUTICS AND SPACE ADMINISTRATION

TECHNICAL NOTE D-984

AERODYNAMIC EFFECTS OF SOME CONFIGURATION VARIABLES ON THE AEROELASTIC CHARACTERISTICS OF LIFTING SURFACES AT MACH NUMBERS FROM 0.7 TO 6.86

By Perry W. Hanson

SUMMARY

Results of flutter tests on some simple all-movable-control-type models are given. One set of models, which had a square planform with double-wedge airfoils with four different values of leading- and trailing-edge radii from 0 to 6 percent chord and airfoil thicknesses of 9, 11, 14, and 20 percent chord, was tested at Mach numbers from 0.7 to 6.86. The bending-to-torsion frequency ratio was about 0.33. The other set of models, which had a tapered planform with single-wedge and double-wedge airfoils with thicknesses of 3, 6, 9, and 12 percent chord, was tested at Mach numbers from 0.7 to 3.98 and a frequency ratio of about 0.42.

The tests indicate that, in general, increasing thickness has a destabilizing effect at the higher Mach numbers but is stabilizing at subsonic and transonic Mach numbers. Double-wedge airfoils are more prone to flutter than single-wedge airfoils at comparable stiffness levels. Increasing airfoil bluntness has a stabilizing effect on the flutter boundary at supersonic speeds but has a negligible effect at subsonic speeds. However, increasing bluntness may also lead to divergence at supersonic speeds.

Results of calculations using second-order piston-theory aerodynamics in conjunction with a coupled-mode analysis and an uncoupled-mode analysis are compared with the experimental results for the sharp-edge airfoils at supersonic speeds. The uncoupled-mode analysis more accurately predicted the flutter characteristics of the tapered-planform models, whereas the coupled-mode analysis was somewhat better for the square-planform models. For both the uncoupled- and coupled-mode analyses, agreement with the experimental results improved with increasing Mach number. In general, both methods of analysis gave unconservative results with respect to the experimental flutter boundaries.

INTRODUCTION

The stringent operating requirements being placed on present high-speed aircraft and missiles will very likely be accentuated in the future, resulting in the design of structures of maximum efficiency with a minimum of weight to sustain a given load. The resulting relatively flexible structures can very easily invite aeroelastic instabilities such as flutter and divergence. Parameters that determine the aeroelastic characteristics of these vehicles must be considered over the entire speed range from subsonic to transonic through supersonic and hypersonic. The extremely high speeds involved are dictating major changes in airfoil configurations, particularly on missile lifting and control surfaces. Wedge and double-wedge airfoils are being more widely used and airfoils with blunt leading edges are also coming into greater use in order to satisfy aerodynamic-heating requirements. Therefore, among the aeroelastic parameters which are becoming increasingly important are the airfoil thickness, shape, and bluntness.

These parameters and others have been investigated analytically at the higher Mach numbers (e.g., refs. 1 and 2), and some experimental investigations of single-wedge airfoils have been carried out at high Mach numbers (for example, refs. 3 and 4) for specific surfaces. The results of a few experimental trend studies at high Mach numbers are available. Reference 5 presents results of an investigation of the aerodynamic effect of thickness on the flutter characteristics of some simple rectangular-planform models having double-wedge airfoils tested at a Mach number of 7.2. Reference 6 presents results of tests at a Mach number of 7.0 of some delta all-movable-control models having leading-edge sweep angles from 60° to 80° and both single-wedge and double-wedge airfoil sections. The effects of airfoil thickness on the transonic flutter characteristics of some unswept rectangular-planform wings with circular-arc airfoil sections and some swept tapered-planform wings with NACA 65A-series airfoils are presented in reference 7 for Mach numbers from 0.70 to 1.10. In reference 8, the effect of thickness on the flutter characteristics of a simple rectangular-planform wing having a beveled-leading-edge flat-plate airfoil, a double-wedge airfoil, and a flat plate with a leading-edge radius of 2 percent chord was investigated at a Mach number of 3.0.

It will be noted that most of the investigations have dealt with the effect of thickness or airfoil shape or both together at a particular Mach number or at best over a limited Mach number range. It is desirable to study the effects of airfoil thickness, shape, and bluntness over a wide range of Mach numbers from transonic to hypersonic velocities. The purpose of this investigation was to determine the effects of these parameters on the aeroelastic characteristics of some simple all-movable-control-type surfaces over a wide range of Mach numbers (0.7 to 6.86)

from transonic to hypersonic velocities. The models used were kept as simple as possible in order that the structural properties and other parameters not included in the study could be more easily controlled. Basically, two types of models were tested: an unswept, square-planform, shaft-mounted model and an unswept, tapered-planform, leaf-spring-mounted model. The thickness of the square-planform models ranged from 9 to 20 percent chord and the bluntness range extended from 0- to 6-percent-chord leading- and trailing-edge radii. The thickness of the tapered models ranged from 3 to 12 percent chord for the double-wedge airfoils and from 6 to 12 percent chord for the single-wedge airfoil.

SYMBOLS

a	free-stream speed of sound, ft/sec
b	wing semichord, in.
$b_{.75}$	wing semichord at 0.75-semispan station, based on exposed semispan, measured parallel to airstream, in.
c	local chord, in.
d	thickness of square-model steel core and shaft, in. (see fig. 1)
e	streamwise distance from leading edge of reflection plane to leading edge of square model, in.
f_b	tapered-model bending frequency (pitch degree of freedom restrained), cps
f_f	flutter frequency, cps
f_n	natural frequency of nth mode (n = 1, 2, and 3), cps
f_θ	tapered-model pitching frequency (bending degree of freedom restrained), cps
g	acceleration due to gravity
h	perpendicular distance from tunnel wall to square-model root, in.
I_b	mass moment of inertia about bending or clamp axis of model including panel mounting block, shaft, and screws (includes free portion of shaft of square models), in-lb-sec^2

I_m mass moment of inertia about pitch axis of all moving parts of tapered-model mounting system, in-lb-sec^2

I_θ mass moment of inertia about pitch axis of model including all moving parts of mounting system (square-model shaft neglected), in-lb-sec^2

l length of semispan model, measured normal to root chord and stream direction, in.

M Mach number

m mass of portion of square model exposed to airstream, lb-sec^2/in.

q dynamic pressure, lb/sq ft

R stiffness-altitude parameter, $\frac{1}{6}\frac{\pi t f_2}{a}\sqrt{\mu}$

r square-model leading- and trailing-edge radius, in.

r_θ radius of gyration of model and mount assembly, referred to pitch axis, $\sqrt{\frac{I_\theta g}{W_T(b.75)^2}}$ for tapered models and $\sqrt{\frac{I_\theta}{mb^2}}$ for square models, in./in.

t model maximum thickness (maximum thickness is at 0.50c for double-wedge airfoils and at 1.0c for wedge airfoils), in.

W weight of tapered model including panel mounting block, shaft, and screws, lb

W_B weight of tapered-model panel mounting block, shaft, and screws, lb

W_T weight of tapered model and moving portion of tapered-model mounting system, $W - W_B + W_m$

W_m weight of entire moving portion of tapered-model mounting system, lb

x chordwise station, measured parallel to root chord from leading edge, in.

y spanwise station, measured perpendicular to root chord from the root, in.

z vertical displacement of vibrating model from equilibrium position

δ slope of straight-line portion of square airfoil surfaces, deg

μ nondimensional mass ratio parameter (ratio of mass of exposed model to mass of volume of test medium contained in solid generated by revolving each chord about its midpoint, length of solid being wing semispan)

ρ test-medium density, slugs/cu ft

Subscripts:

exp experimental

th theoretical

APPARATUS AND TEST PROCEDURE

Description of Wind Tunnels

The tests on the semispan wall-mounted models were conducted in the Langley 2-foot transonic aeroelasticity tunnel for the Mach number range from 0.7 to 1.17, in the Langley 9- by 18-inch supersonic aeroelasticity tunnel for the Mach number range from 1.3 to 3.98, and in the Langley hypersonic aeroelasticity tunnel and the Langley 11-inch hypersonic tunnel for Mach numbers 6.83 and 6.86, respectively.

The Langley 2-foot transonic aeroelasticity tunnel is a slotted-throat single-return wind tunnel equipped to use either air or Freon-12 as a test medium. All the present tests were made with Freon-12. The tunnel is of the continuous-operation type, powered by a motor-driven fan. Both test-section Mach number and density are continuously controllable.

The Langley 9- by 18-inch supersonic aeroelasticity tunnel is a fixed-nozzle air blowdown-type wind tunnel exhausting into a vacuum sphere. The nozzle configurations used in this investigation gave Mach numbers of 1.30, 1.64, 2.00, 2.55, 3.00, and 3.98. At each Mach number the test-section density varies continuously to a controlled maximum.

The Langley hypersonic aeroelasticity tunnel and the Langley 11-inch hypersonic tunnel are both fixed-nozzle blowdown-type wind tunnels exhausting into a vacuum sphere. The nozzle configuration used in the Langley hypersonic aeroelasticity tunnel with helium as a test medium gave a Mach number of 6.83. This tunnel has an 8-inch-diameter test section. The nozzle configuration used in the Langley 11-inch hypersonic tunnel with air as a test medium gave a Mach number of 6.86. The characteristics of this tunnel are given in reference 9.

Test Procedure

The determination of a typical flutter point in the Langley 2-foot transonic aeroelasticity tunnel proceeded as follows: With the tunnel evacuated to a low stagnation pressure, the compressor speed (Mach number) was increased until flutter occurred or until maximum permissible speed was reached. If flutter did not occur the compressor speed was reduced and the test-section density was increased by a small amount. The Mach number was slowly increased again at the higher density. When flutter occurred the test-section dynamic pressure and Mach number were rapidly decreased by actuating a "flutter stopper" (a spoiler in the diffuser section of the tunnel). The actuation of the flutter stopper also locked the tunnel instruments so that the tunnel conditions necessary to describe completely the flutter point could be recorded after precautions had been taken to save the model. The compressor speed was then decreased to a point well below the flutter condition and the spoiler was retracted. At this time the tunnel density was increased by a small amount, after which the test-section Mach number was slowly increased until the next flutter condition occurred. This same procedure was repeated several times, completely defining the flutter region within the operational limits of the tunnel.

The test procedure used for all three blowdown tunnels was more straightforward and essentially the same. With a nozzle installed to give the desired Mach number, the tunnel was evacuated to a very low pressure. A control valve upstream of the test section was opened and the density of the flow was allowed to increase at constant Mach number until flutter occurred. Tunnel conditions throughout the run were recorded on a recording oscillograph.

During each flutter condition the outputs from the bending and torsion resistance-wire strain gages mounted on the model shaft or mounting springs were recorded on a recording oscillograph. From these oscillograph records the flutter frequencies were determined. The first two or three natural frequencies were obtained for each model before and after each tunnel test to determine whether or not the model had been damaged.

MODELS

The semispan models tested were of two general types: one type (hereinafter referred to as square models) was simple, square-planform, shaft-mounted, all-movable-control-type models. These models were designed to study the effect of bluntness on the aeroelastic properties. The other general type (hereinafter referred to as tapered models) was spring mounted in two degrees of freedom and had a ratio of tip chord to root chord of 0.5. These models were designed primarily to study airfoil shape and thickness effects.

Configuration and Construction

Square models.- All the square models had panel aspect ratios of 1.0, zero sweep, and a 4-inch span. The models were supported by a shaft of rectangular cross section which was 3 inches long (1 inch of the shaft length was used for the clamping surface). Shafts having three different thicknesses were used in order to have models with three different levels of stiffness. The airfoils of this series of models were all double-wedge airfoils although some had different leading- and trailing-edge bluntnesses. The method of designating the different model configurations is shown in table I along with the corresponding model and shaft thickness, leading- and trailing-edge radii, and slopes of the straight portions of the airfoils.

The method of construction is shown in figure 1. Essentially, the square models consisted of a stainless-steel core with integral shaft to which lightweight balsa wood was bonded to give the different airfoil shapes. The metal cores were drilled and weighted with lead in such a manner that the inertial properties and frequency ratios of the models having different airfoils and stiffnesses were very nearly constant.

Figure 2 shows how these models were mounted and figure 3 shows the methods used in the various tunnels to reduce tunnel-boundary-layer effects. Reflection planes were used in the supersonic and hypersonic tunnels and a semicircular fairing was used in the transonic tunnel. Reflection plane 1 was used in the Langley hypersonic aeroelasticity tunnel (helium flow) and the Langley 11-inch hypersonic tunnel (air flow) before it was discovered that boundary-layer buildup along the long reflection plane was causing a shock to impinge on the model. Reflection plane 2 was constructed so that the distance from the leading edge of the reflection plane to the leading edge of the model was reduced from 3.3 inches to 1.0 inch; thus, boundary-layer buildup was limited on the reflection plane. The models were tested again in the hypersonic aeroelasticity tunnel and although there was little difference

in the data obtained, reflection plane 2 was used in all subsequent tests in the hypersonic aeroelasticity tunnel.

Tapered models.- All the tapered models had a panel aspect ratio of 1.493, a taper ratio of 0.50, zero sweep, a 6.50-inch semispan, and a 5.80-inch root chord as shown in figure 4. All models were mounted on leaf springs (fig. 5) in a manner permitting pitch and flapping freedom. Double-wedge airfoils having maximum thicknesses of 3, 6, 9, and 12 percent chord and single-wedge airfoils having maximum thicknesses of 6, 9, and 12 percent chord were tested. In the tapered-model configuration designation, the first number indicates the maximum airfoil thickness in percent chord, the D or W indicates a double-wedge or single-wedge airfoil, and the number 1, 2, or 3 indicates the spring configuration used; thus, model 3D-1 indicates a 3-percent-thick double-wedge airfoil using springs 0.027 inch thick. (The spring thicknesses are shown in fig. 5.)

L
1
6
2
6

The various airfoil shapes were obtained, as shown in figure 4, by adding properly contoured plastic foam to a 3-percent-thick, solid-aluminum, double-wedge-airfoil core. The center of gravity of all the models was kept in the same location, and variations of other inertial properties of the models were minimized by ballasting the models with lead strips along the trailing edges.

Figure 5 shows the method of mounting the tapered models. Bending and pitch springs of 3 different thicknesses were used to give stiffnesses such that flutter points could be obtained throughout the Mach number range investigated.

Figure 6(a) shows the method of mounting the models on a reflection plane outside the boundary layer in the Langley 9- by 18-inch supersonic aeroelasticity tunnel and figure 6(b) shows how the models were mounted through an opening in the semicircular fairing in the Langley 2-foot transonic aeroelasticity tunnel.

The tapered models were not tested in the Langley hypersonic aeroelasticity tunnel due to their relatively large span. Hence the flutter boundaries for these models were defined only up to a Mach number of 3.98.

Physical Properties

Square models.- The pitch axis of all the square models was at the 35-percent-chord position with the panel center of gravity at 53.5 percent chord and 50 percent semispan. The center of gravity did not deviate from model to model by more than 1/2 percent of the

chord. These models were designed to have a mass equal to 450×10^{-6} lb-sec^2/in., a mass moment of inertia about the pitch axis of 825×10^{-6} in-lb-sec^2, and a "flapping" mass moment of inertia about the shaft clamp axis of $7,900 \times 10^{-6}$ in-lb-sec^2. Few models varied by more than 4 percent from these design values. Where slightly higher variations occurred in one or more of the parameters, the data points for these models were checked by testing other models of like configuration. The actual values of mass and inertia of the various models are shown in table II along with the test results. The first two natural vibration frequencies also are shown in table II.

The first two natural vibration mode shapes of the square models were determined experimentally for each of the three shaft stiffnesses. This was done by forcing the model in one of its natural vibration modes by means of an interrupted air jet to a sufficient amplitude to allow mechanical measurement of the amplitude at the four corners of the all-movable control. It was assumed that for the first two modes the model panel did not deform and that all the flexing was done in the mounting shaft. This assumption was verified qualitatively by viewing the models vibrating at large amplitudes under a stroboscopic light. These mode shapes, normalized on the maximum deflection, are presented in table III along with the third natural vibration mode frequency range and a typical node line for the three different shaft stiffnesses.

Tapered models.- All the tapered models had the pitch axis at 37 percent of the root chord and a bending axis 9 percent of the exposed semispan inboard of the root chord. The panel centers of gravity of all the tapered models were held to a position 2.50 inches from the root and 2.58 inches from the leading edge measured along the local chord parallel to the root chord. The tapered models were designed to have a weight of 0.310 pound, and a pitching mass moment of inertia about the pitch axis of $1,800 \times 10^{-6}$ in-lb-sec^2, the mounting system being included. The actual weights, inertias, and radii of gyration of the models and mounting system are shown in table IV along with the first two experimentally determined uncoupled frequencies for the three spring stiffnesses used. The panel mass distribution was calculated by assuming the density of the aluminum core and plastic foam to be uniform. This distribution is presented in table V.

The natural vibration mode shapes for the seven tapered models were determined by the experimental method of reference 10 for spring series 1. It was assumed that the mode shapes would not change substantially with the slight change in stiffness caused by using spring configuration 2 or 3 instead of 1. These representative mode shapes are presented in table VI. Typical node lines for the tapered models are presented in figure 7. Only the first two natural vibration modes were determined for each of the airfoil configurations except that the third mode was determined for the 9-percent-thick wedge.

RESULTS AND DISCUSSION

General

The basic data obtained from tests on the square models and the tapered models are presented in tables VII and VIII, respectively. The results are presented in figures 8 to 15 in the form of stability boundaries in terms of the variation with Mach number of the stiffness-altitude parameter $R = \frac{1}{6}\frac{\pi b f_2}{a}\sqrt{\mu}$ (for the tapered models, b is taken at 0.75 semispan) and the flutter frequencies. The parameter R depends upon the physical properties of the wing - in particular, the torsional stiffness - and upon the atmosphere in which the wing operates. Its value increases as either altitude or stiffness increases. When R is plotted against Mach number, curves for constant dynamic pressure will appear as radial lines through the origin. The stable region is above the boundary. For the untapered models the mass-ratio parameter μ is defined as the ratio of the mass of the model (excluding the shaft) to the mass of the volume of the test medium contained in the right circular cylinder whose height is the model semispan and whose diameter is equal to the model chord. For the tapered series the mass ratio is defined in the same manner except the model mass includes the portion of the mounting system that moves in the flapping mode, and the volume of the test medium is that which is contained in the conical frustum whose height is equal to the model semispan and whose bases have diameters equal to the model root and tip chords, respectively.

L 1626

Square Models

Experimental.- From the experimental results shown in figure 8 of tests on the square models it can be seen that in the subsonic speed range airfoil bluntness has little effect on the flutter boundary. In the immediate vicinity of a Mach number of 1, the blunter models appear to flutter at a slightly lower density than the sharper models (the flutter boundary is higher) but this trend is reversed just above a Mach number of 1 and increasing bluntness from 0-percent-chord radius to 1- and 3-percent-chord radii considerably raises the flutter density (lowers the flutter boundary) for the rest of the Mach number range. The model with 6-percent-chord radius warrants special consideration. The flutter boundary drops sharply in the vicinity of a Mach number of 1; thus, a much higher dynamic pressure is required for flutter than for the sharper models. However, at a Mach number of 1.3, the boundary is approximately equal to that of the airfoil with a 1-percent-chord radius. For verification, three different models were tested at this Mach number. At $M = 1.64$ no flutter was obtained - instead, the models

diverged - and this held true for the rest of the Mach number range. The long-dashed line in figure 8 indicates the divergence boundary. In most cases, the divergence was quite abrupt with the model striking the reflection plane less than 0.1 second after the first observable displacement. At M = 3.98, however, the divergence occurred somewhat more slowly and the extreme limits between start and completion of divergence are indicated in figure 8 by the short-dashed line between two solid data points. In an attempt to determine if the divergence was due to bluntness or thickness, a model was tested at M = 3.0 that had a 6 percent leading and trailing edge but was only 12 percent thick instead of 20 percent thick. The model still diverged but at a higher dynamic pressure. A shortage of models precluded extending this test to other Mach numbers.

Also shown in figure 8 are the experimental results of testing square models all having sharp leading and trailing edges but having three different thicknesses. It may be seen that increasing the thickness from 9 to 14 and 20 percent chord raised the flutter boundaries with the largest change occurring in the low supersonic Mach number range when the thickness was increased from 14 percent chord to 20 percent chord.

At M = 6.86 and 6.83, tests that were made on some airfoils with 0- and 1-percent-chord radius tested on reflection plane 1 are indicated in figure 8 with a tick on the respective symbols. These points are included to show the correlation between testing in helium at M = 6.83 and in air at M = 6.86. It would appear that for the sharp-edge airfoils there is little difference between testing in helium and testing in air. For the airfoil with 1-percent-chord radius, it appears that the test in helium indicates a slightly higher boundary than the test in air.

An indication of the experimental "scatter" is shown at several Mach numbers where attempts were made to repeat a particular test.

In summary, for square models having frequency ratios, center-of-gravity location, and pitch-axis location similar to those used in the test, bluntness appears to be stabilizing at supersonic speeds from the flutter standpoint except that extremes in bluntness may lead to divergence problems. Likewise, in the supersonic regime, thickness has a destabilizing effect on the flutter boundary.

Theoretical.- The calculated flutter boundaries are presented for the square models with sharp-edge airfoils for the supersonic speed range. Two-degree-of-freedom flutter calculations were made for these models using the first two coupled or uncoupled flapping and pitching modes in conjunction with the second-order piston theory of reference 11.

The coupled modes and frequencies used in the analysis were experimentally determined as described in the section "Physical Properties." The procedure used for the coupled-mode analysis followed closely that of reference 12. The calculations for the uncoupled modes and frequencies were based on the assumption that the exposed section of the model vibrated as a rigid body while the elastic deformation took place in the shaft. It was also assumed that the panel mass was uniform over the span, which was very nearly the case. The results of these calculations are presented in figures 9, 10, and 11. In figure 9(a) the stiffness-altitude parameter, as calculated by using the uncoupled-mode analysis, is plotted against Mach number for the three airfoils under discussion. Figure 9(b) shows the variation of the stiffness-altitude parameter with Mach number predicted by the coupled-mode analysis, and figures 10 and 11 show the agreement of the calculated stiffness-altitude parameter and flutter frequencies with the experimental values. From figure 9(a) it may be seen that the uncoupled-mode analysis correctly predicts the experimentally determined destabilizing effect of thickness of the sharp-edge airfoils. The coupled-mode analysis (fig. 9(b)) predicts the destabilizing effect of increasing thickness from 9 percent chord to 20 percent chord but shows no difference between the 9- and 14-percent-thick airfoils. This analysis also predicts flutter at generally lower densities than the uncoupled-mode analysis. The ratios of the theoretical stiffness-altitude parameter to the experimental values presented in figures 10(a) and 10(b) show that the coupled-mode analysis agrees better than the uncoupled-mode analysis with the experimental values over most of the Mach number range. The ratios of theoretical flutter frequency to experimental frequency are presented in figures 11(a) and 11(b) for the uncoupled- and coupled-mode analysis, respectively. The coupled-mode analysis more accurately predicted the flutter frequencies than did the uncoupled-mode analysis, although neither method gave really good results.

These discrepancies between theoretical and experimental values may be in part attributed to the fact that the models have a very low aspect ratio with attendant relatively large tip effects not accounted for by the theory, particularly at the lower supersonic Mach numbers. Also, it has been shown in reference 5 that for very similar models, the location of the pitch axis influenced greatly the agreement between second-order piston theory (using uncoupled modes) and the experimental values of the stiffness-altitude parameter.

Tapered Models

Experimental.- Figures 12(a) and 12(b) show the experimental results of the tests on the tapered double-wedge and single-wedge airfoils, respectively. For the case of the double-wedge airfoil at subsonic speeds the effect of increasing thickness is to increase the

stability. However, above $M = 1.15$ this trend is reversed so that thickness is destabilizing throughout the rest of the Mach number range. It will be noted in figure 12(a) that just below $M = 1.0$ an irregularity is evident in the flutter-boundary curves for the 9- and 12-percent-thick airfoils. In order to investigate the cause of this, small tufts of string were glued to the surfaces of the models and high-speed motion pictures were taken of the models as the flutter condition was approached. It was observed that the boundary layer was separating from the 9- and 12-percent-thick models just downstream of the midchord prior to flutter. This phenomenon occurred over a range of Mach numbers that roughly coincided with the irregular flutter boundaries for these models.

In figure 12(b) the results of tests on the single-wedge airfoils show that the 6-percent-thick airfoil is more susceptible to flutter than the 9- or 12-percent-thick airfoils throughout the Mach number range. As in the case of the double-wedge airfoils, below approximately $M = 1.15$, thickness is stabilizing when the thickness is increased from 6 percent chord to 9 percent chord. However, for the single-wedge airfoil there appears to be no appreciable effect of increasing thickness from 9 to 12 percent chord. Unlike the double-wedge airfoils, the single-wedge airfoils do not exhibit clear-cut thickness effects at supersonic speeds. Generally, it would appear that the 12-percent-thick single wedge is slightly more susceptible to flutter than the 9-percent-thick single wedge but not appreciably so until $M = 3.98$.

In comparing the single-wedge airfoils with the double-wedge airfoils it is seen that the boundaries of the 3-percent-thick double wedge and the 6-percent-thick single wedge are almost alike except in the transonic region where the single-wedge airfoil is much more susceptible to flutter than the double-wedge airfoil. In the supersonic region, with the exception of these airfoils, the double-wedge airfoils are seen to be more susceptible to flutter than the single-wedge airfoils.

Theoretical.- Theoretical flutter boundaries for the tapered models were calculated by using both uncoupled- and coupled-mode two-degree-of-freedom analyses with second-order piston-theory aerodynamics. The first two uncoupled modes used in the analysis were determined experimentally by restraining the model in the unwanted degree of freedom and physically measuring the vibrating deflection at the four corners of the panel. (The panel was assumed to be rigid with all flexing taking place in the springs.) These measurements, in addition to viewing the vibrating model under a stroboscopic light, indicated it would be reasonable to assume that the torsion mode consisted of a unit twist along the entire span and the bending mode was the straight line given by $z = \frac{1}{12.5}\left(1.0 + 1.15\,\frac{y}{l}\right)$. The uncoupled frequencies associated

with these modes are given in table IV. (The same uncoupled mode shape was used for all models.) The experimentally measured coupled mode shape and frequencies used in the coupled-mode analysis are shown in table VI. The distributed mass properties used in all the calculations are shown in table V.

The results of these calculations are presented in figures 13, 14, and 15. The variation with Mach number of the theoretical stiffness-altitude parameter obtained from both methods for the double-wedge airfoils is shown in figure 13(a). The uncoupled-mode analysis predicts the destabilizing effect of airfoil thickness over the Mach number range. The coupled-mode analysis is more conservative and the thickness effects are not as well defined. For the single-wedge airfoils (fig. 13(b)) the uncoupled-mode analysis gives more conservative results than the coupled-mode analysis. It shows little effect of thickness (as was indicated by the experimental results). Also, the effect shown is such that the flutter boundary for the 12-percent-thick airfoil falls between those of the 6- and 9-percent-thick airfoils. It will be recalled that the experimental results indicated this trend also. Both the coupled- and uncoupled-mode analyses give practically the same flutter boundary for the 6-percent-thick single-wedge airfoil.

L
1
6
2
6

The agreement of the results of the two methods of analysis with the experimental stiffness-altitude parameter is presented in figure 14. It is seen that for both the single-wedge and double-wedge airfoils the uncoupled-mode analysis agrees better with the experimental values than does the coupled-mode analysis, particularly at the higher Mach numbers. Figures 15(a) and 15(b) show the agreement between experimental flutter frequencies and those calculated by using the uncoupled-mode analysis for the double-wedge and single-wedge airfoils, respectively. A similar comparison for the coupled-mode analysis for the two airfoil sections is shown in figures 15(c) and 15(d). From these figures it can be seen that the uncoupled-mode analysis comes closer to predicting the experimental flutter frequencies for the single-wedge airfoils but there is not much difference between the two methods in the degree of accuracy in predicting flutter frequencies of the double-wedge models.

CONCLUDING REMARKS

Tests on square-planform, all-movable-control-type models having leading- and trailing-edge radii from 0 to 6 percent chord and airfoil thicknesses from 9 to 20 percent chord over the Mach number range from 0.7 to 6.86 and on tapered-planform models with single-wedge and double-wedge airfoil of thicknesses from 3 to 12 percent chord over the Mach number range from 0.7 to 3.98 indicate a definite effect of airfoil bluntness and thickness on the aeroelastic characteristics.

For the parameter ranges of the investigation, the tests indicate that in the supersonic speed range the effect of thickness is destabilizing, while in the subsonic range it may be slightly stabilizing, for both single-wedge and double-wedge airfoils.

The double-wedge airfoils fluttered at a lower density than single-wedge airfoils of comparable stiffness. The effect of airfoil thickness on the flutter characteristics of the single-wedge airfoils was not as great as it was on the double-wedge airfoils.

Increasing airfoil bluntness, within limits, had a stabilizing effect on the flutter characteristics of the square models in the supersonic speed range but had a negligible effect in the subsonic range. Increasing airfoil bluntness to 6-percent-chord leading- and trailing-edge radii led to divergence at Mach numbers greater than 1.3.

Flutter calculations using second-order piston-theory aerodynamics in conjunction with an uncoupled-mode analysis and a coupled-mode analysis indicated that in general the uncoupled-mode analysis more accurately predicted the flutter characteristics of the tapered models, whereas the coupled-mode analysis was somewhat better for the square models. For both the uncoupled and coupled-mode analyses, agreement with the experimental results improved with increasing Mach number. In general, both methods of analysis gave unconservative results with respect to the experimental flutter boundaries.

Langley Research Center,
National Aeronautics and Space Administration,
Langley Air Force Base, Va., September 14, 1961.

REFERENCES

1. Chawla, Jagannath P.: Aeroelastic Instability at High Mach Number. Jour. Aero. Sci., vol. 25, no. 4, Apr. 1958, pp. 246-258.

2. Morgan, Homer G., Runyan, Harry L., and Huckel, Vera: Theoretical Considerations of Flutter at High Mach Numbers. Jour. Aero. Sci., vol. 25, no. 6, June 1958, pp. 371-381.

3. Gibson, Frederick W., and Mixson, John S.: Flutter Investigation at a Mach Number of 7.2 of Models of the Horizontal- and Vertical-Tail Surfaces of the X-15 Airplane. NASA MEMO 4-14-59L, 1959.

4. Lauten, William T., Jr., Levey, Gilbert M., and Armstrong, William O.: Investigation of an All-Movable Control Surface at a Mach Number of 6.86 for Possible Flutter. NACA RM L58B27, 1958.

5. Morgan, Homer G., and Miller, Robert W.: Flutter Tests of Some Simple Models at a Mach Number of 7.2 in Helium Flow. NASA MEMO 4-8-59L, 1959.

6. Miller, Robert W., and Hannah, Margery E.: Flutter Investigation of 60° to 80° Delta-Planform Surfaces at a Mach Number of 7.0. NASA TM X-325, 1960.

7. Doggett, Robert V., Jr., Rainey, A. Gerald, and Morgan, Homer G.: An Experimental Investigation of Aerodynamic Effects of Airfoil Thickness on Transonic Flutter Characteristics. NASA TM X-79, 1959.

8. Martuccelli, John R.: Flutter Model Tests at Mach Numbers 1.5-5.0. WADC Tech Rep. 59-407, U.S. Air Force, Sept. 1959.

9. McLellan, Charles H., Williams, Thomas W., and Beckwith, Ivan E.: Investigation of the Flow Through a Single-Stage Two-Dimensional Nozzle in the Langley 11-Inch Hypersonic Tunnel. NACA TN 2223, 1950.

10. Hanson, Perry W., and Tuovila, W. J.: Experimentally Determined Natural Vibration Modes of Some Cantilever-Wing Flutter Models by Using an Acceleration Method. NACA TN 4010, 1957.

11. Ashley, Holt, and Zartarian, Garabed: Piston Theory - A New Aerodynamic Tool for the Aeroelastician. Jour. Aero. Sci., vol. 23, no. 12, Dec. 1956, pp. 1109-1118.

12. Morgan, Homer G., Huckel, Vera, and Runyan, Harry L.: Procedure for Calculating Flutter at High Supersonic Speed Including Camber Deflections, and Comparison With Experimental Results. NACA TN 4335, 1958.

TABLE I.- MODEL DESIGNATIONS AND AIRFOIL DIMENSIONS

FOR SQUARE MODELS

Model designation (a)	r, in.	t, in.	d, in.	δ, deg
0- 9-33-( )	0	0.35	0.033	5.0
0-14-33-( )	0	.56	.033	8.0
0-20-33-( )	0	.80	.033	11.3
1-11-33-( )	.04	.43	.033	5.0
3-14-33-( )	.12	.56	.033	5.0
6-20-33-( )	.24	.80	.033	5.0
0- 9-47-( )	0	.35	.047	5.0
0-14-47-( )	0	.56	.047	8.0
0-20-47-( )	0	.80	.047	11.3
1-11-47-( )	.04	.43	.047	5.0
3-14-47-( )	.12	.56	.047	5.0
6-20-47-( )	.24	.80	.047	5.0
6-12-47-( )	.24	.48	.047	0
0- 9-65-( )	0	.35	.065	5.0
0-14-65-( )	0	.56	.065	8.0
0-20-65-( )	0	.80	.065	11.3
1-11-65-( )	.04	.43	.065	5.0
3-14-65-( )	.12	.56	.065	5.0
6-20-65-( )	.24	.80	.065	5.0

[a]The first number in the designation represents the leading- and trailing-edge radius in percent chord; the second group of numbers represents the nominal maximum thickness in percent chord; the third group of numbers represents the thickness of the shaft in thousandths of inches; the last group is the model number in a particular airfoil configuration.

TABLE II.- PHYSICAL PROPERTIES OF SQUARE MODELS

Model	m, $\frac{\text{lb-sec}^2}{\text{in.}}$	I_θ, in-lb-sec^2	I_b, in-lb-sec^2	f_1, cps	f_2, cps
0- 9-33-2	458 × 10^6	816 × 10^6	8,090 × 10^6	12.2	42.3
0- 9-47-4	456	813	7,930	20.2	66.2
0- 9-47-3	457	820	7,970	20.0	66.8
0- 9-65-3	461	842	8,055	32.5	103.0
0- 9-65-2	462	843	8,210	31.5	100.8
0- 9-47-5	460	814	8,080	20.4	67.0
0- 9-65-4	455	846	8,120	32.0	103.4
0- 9-65-1	464	838	8,240	31.4	102.4
0- 9-47-1	459	831	7,970	20.2	66.2
0- 9-33-1	457	827	8,067	12.1	41.0
0- 9-47-3	457	820	7,970	20.2	66.1
0- 9-33-3	458	822	8,090	11.3	41.7
0- 9-33-6	457	834	8,067	11.9	42.9
0- 9-33-2	458	816	8,090	11.8	42.4
0- 9-47-2	458	823	7,980	20.5	68.0
0- 9-65-5	457	818	8,400	30.9	101.0
0-14-65-5	456	847	8,277	31.1	100.2
0-14-65-3	456	839	8,277	32.6	105.6
0-14-65-5	456	847	8,277	31.4	100.8
0-14-47-1	448	804	7,785	20.4	70.4
0-14-47-2	440	804	7,690	18.4	66.8
0-14-65-1	458	810	7,922	31.6	105.0
0-20-65-6	447	813	8,247	33.6	111.6
0-20-65-4	443	805	7,695	33.6	109.6
0-20-65-6	447	813	8,247	33.4	111.0
0-20-47-3	445	819	7,738	20.0	69.4
0-20-47-3	445	819	7,738	20.0	69.4
0-20-65-4	443	805	7,695	33.2	111.6
0-20-47-1	435	797	7,630	20.0	70.1
1-11-47-5	459	851	7,960	19.3	66.6
1-11-65-3	451	828	8,018	32.2	101.6
1-11-65-1	454	851	8,020	32.0	102.2
1-11-47-4	465	835	8,053	20.6	69.3
1-11-47-6	463	844	7,968	19.5	65.4
1-11-65-2	461	856	8,140	33.0	104.0

TABLE II.- PHYSICAL PROPERTIES OF SQUARE MODELS - Concluded

Model	m, $\frac{\text{lb-sec}^2}{\text{in.}}$	I_θ, in-lb-sec^2	I_b, in-lb-sec^2	f_1, cps	f_2, cps
1-11-47-1	450×10^6	810×10^6	$7,843 \times 10^6$	20.5	68.4
1-11-33-5	450	832	7,930	12.1	41.0
1-11-47-5	459	851	7,960	19.4	65.6
1-11-33-1	459	835	8,105	11.8	43.4
1-11-33-4	450	832	7,920	11.7	43.2
1-11-47-2	453	827	7,877	19.9	67.6
1-11-47-3	448	819	7,788	20.4	67.4
3-14-47-2	445	827	7,748	20.2	70.0
3-14-65-2	450	838	8,050	32.8	109.4
3-14-47-2	445	827	7,748	20.6	69.6
3-14-65-1	448	814	7,863	32.5	107.2
3-14-47-1	448	812	7,785	20.9	72.8
3-14-65-5	467	860	8,550	31.9	108.0
3-14-65-3	454	837	8,090	33.2	112.2
3-14-47-4	458	835	7,947	20.8	72.6
3-14-33-3	446	834	7,915	12.4	44.2
3-14-33-1	447	836	7,850	12.0	44.0
3-14-47-1	448	812	7,785	20.5	72.4
6-20-47-1	435	802	7,610	20.8	74.4
6-20-47-2	441	813	7,682	20.3	72.0
6-20-65-3	437	788	7,620	34.1	117.5
6-20-65-1	448	793	7,760	32.6	115.0
6-20-47-2	441	813	7,682	19.8	70.0
6-20-65-1	448	793	7,760	32.6	116.0
6-20-47-1	435	802	7,610	20.8	73.7
6-20-65-2	456	820	7,900	32.4	117.6
6-20-65-6	447	813	7,780	34.0	115.0
6-20-47-3	445	827	7,738	20.4	72.6
6-12-47-2	428	797	7,497	20.7	70.6
6-20-33-1	442	836	7,772	12.4	44.2
6-20-47-2	441	813	7,682	20.6	74.0
6-20-47-2	441	813	7,682	20.5	73.6

TABLE III.- MODE SHAPES OF SQUARE MODELS

Mode	Natural frequency, cps	Normalized deflection			
		Root chord		Tip chord	
		Leading edge	Trailing edge	Leading edge	Trailing edge
Shaft thickness, 0.033 in.					
1	12.1	0.16	0.27	0.87	1.00
2	42.7	.54	-.80	1.00	-.56
Shaft thickness, 0.047 in.					
1	20.3	0.16	0.26	0.83	1.00
2	67.4	.46	-.76	1.00	-.58
Shaft thickness, 0.065 in.					
1	32.1	0.16	0.26	0.86	1.00
2	99.8	.43	-.73	1.00	-.61

Mode	Calculated uncoupled mode shapes (all shaft thicknesses)	Uncoupled frequencies, cps, for shaft thickness of -		
		0.033 in.	0.047 in.	0.065 in.
1	$1.0 + 3.736 \frac{y}{l}$	12.9	21.9	35.5
2	1.0	40.0	68.0	110.5

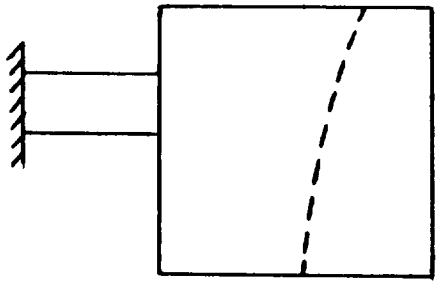

Typical node line for third mode

Shaft thickness, in.	Third mode frequency range, cps
0.033	130 to 155
.047	200 to 235
.065	250 to 260

TABLE IV.- PHYSICAL PROPERTIES OF TAPERED MODEL CONFIGURATIONS

Model configuration	W, lb	I_θ, in-lb-sec^2	I_b, in-lb-sec^2	r_θ^2	f_b, cps	f_θ, cps
3D-1	0.2882	$1,680 \times 10^{-6}$	$8,710 \times 10^{-6}$	0.443	28.3	69.9
-2					26.6	65.7
-3					19.4	46.3
6D-1	0.3507	$1,932 \times 10^{-6}$	$10,660 \times 10^{-6}$	0.447	25.4	62.0
-2					22.0	52.6
-3					17.5	41.0
9D-1	0.3537	$2,205 \times 10^{-6}$	$11,120 \times 10^{-6}$	0.507	24.1	61.1
-2					22.1	51.5
-3					16.8	41.1
12D-1	0.3297	$1,975 \times 10^{-6}$	$9,960 \times 10^{-6}$	0.477	26.8	64.8
-2					23.7	53.0
-3					18.3	42.8
6W-1	0.2757	$1,615 \times 10^{-6}$	$8,160 \times 10^{-6}$	0.438	28.0	71.7
-2					26.3	59.1
-3					19.5	47.0
9W-1	0.2944	$1,774 \times 10^{-6}$	$8,860 \times 10^{-6}$	0.461	27.8	67.1
-2					25.5	56.5
-3					19.3	44.1
12W-1	0.2857	$1,686 \times 10^{-6}$	$8,610 \times 10^{-6}$	0.447	26.6	68.6
-2					25.8	55.5
-3					19.2	44.9

W_m, lb 0.1960
W_B, lb 0.0377
I_m, in-lb-sec^2 . . . . . 203×10^{-6}
Center of gravity, in. from root 2.50
Center of gravity, in. from leading edge 2.58
Pitch axis, in. from leading edge at root 2.16

TABLE V.- COMPUTED MASS DISTRIBUTION OF TAPERED MODELS

Model	Chordwise mass distribution at root chord, slugs/sq ft (a)		Mass of lead ballast at a distance y (in ft) from root, slugs/ft (b)	Location of lead ballast center of gravity, $\frac{x}{c}$
	$\frac{x}{c} = 0$ to $\frac{x}{c} = 0.5$	$\frac{x}{c} = 0.5$ to $\frac{x}{c} = 1.0$		
3D	$0.1753\ \frac{x}{c}$	$0.1753 - 0.1753\ \frac{x}{c}$	$\left[1.325 - 1.218y\right]10^{-4}$	0.95
6D	$0.2223\ \frac{x}{c}$	$0.2223 - 0.2223\ \frac{x}{c}$	$\left[1.555 - 1.437y\right]10^{-4}$	0.95
9D	$0.2270\ \frac{x}{c}$	$0.2270 - 0.2270\ \frac{x}{c}$	$\left[1.532 - 1.408y\right]10^{-4}$	0.95
12D	$0.2060\ \frac{x}{c}$	$0.2060 - 0.2060\ \frac{x}{c}$	$\left[1.522 - 1.400y\right]10^{-4}$	0.95
6W	$0.1675\ \frac{x}{c}$	$0.1575 - 0.1475\ \frac{x}{c}$	$\left[0.680 - 0.626y\right]10^{-4}$	1.00
9W	$0.1733\ \frac{x}{c}$	$0.1562 - 0.1391\ \frac{x}{c}$	$\left[0.768 - 0.708y\right]10^{-4}$	1.00
12W	$0.1705\ \frac{x}{c}$	$0.1588 - 0.1471\ \frac{x}{c}$	$\left[0.836 - 0.771y\right]10^{-4}$	1.00

[a]The tabulated mass distribution is for the root chord (y = 0). To obtain mass distribution along any other chord, multiply these values by $c/5.8$.

[b]Mass of lead ballast is considered concentrated at the center of gravity of the lead ballasting strips.

TABLE VI.- REPRESENTATIVE COUPLED MODE SHAPES OF TAPERED MODELS

[Deflections normalized on maximum deflection; considered positive when deflected wing is above static position]

(a) Model 3D

$\frac{x}{c}$	Normalized deflection at y/l =						
	0	0.15	0.35	0.55	0.75	0.85	1.00
f_1 = 27.0 cps							
0	0.056	0.161	0.329	0.503	0.680	0.779	0.920
.25	.094	.202	.368	.536	.713	.812	.944
.50	.132	.239	.398	.568	.738	.831	.960
.75	.186	.290	.440	.600	.764	.854	.984
1.00	.234	.334	.479	.632	.790	.876	1.000
f_2 = 79.4 cps							
0	-0.667	-0.700	-0.722	-0.756	-0.780	-0.790	-0.803
.25	-.256	-.311	-.367	-.434	-.500	-.534	-.581
.50	.167	.089	0	-.109	-.218	-.271	-.360
.75	.578	.478	.360	.216	.072	-.008	-.133
1.00	1.000	.876	.722	.538	.355	.253	.089

(b) Model 6D

$\frac{x}{c}$	Normalized deflection at y/l =						
	0	0.15	0.35	0.55	0.75	0.85	1.00
f_1 = 23.0 cps							
0	0.045	0.170	0.348	0.520	0.694	0.784	0.922
.25	.100	.225	.388	.549	.718	.804	.937
.50	.157	.272	.430	.582	.746	.828	.956
.75	.220	.326	.468	.615	.772	.852	.981
1.00	.267	.369	.505	.648	.796	.874	1.000
f_2 = 69.1 cps							
0	-0.648	-0.660	-0.680	-0.700	-0.723	-0.735	-0.750
.25	-.235	-.271	-.327	-.383	-.441	-.471	-.524
.50	.182	.106	.007	-.091	-.191	-.236	-.318
.75	.600	.484	.335	.194	.059	-.009	-.106
1.00	1.000	.860	.855	.480	.303	.218	.100

TABLE VI.- REPRESENTATIVE COUPLED MODE SHAPES OF TAPERED MODELS - Continued

(c) Model 9D

$\frac{x}{c}$	Normalized deflection at y/l =						
	0	0.15	0.35	0.55	0.75	0.85	1.00
f_1 = 22.5 cps							
0	0.056	0.199	0.372	0.558	0.742	0.836	0.968
.25	.107	.235	.410	.586	.761	.851	.972
.50	.156	.278	.442	.611	.774	.860	.978
.75	.203	.320	.476	.636	.790	.874	.990
1.00	.245	.357	.508	.660	.808	.887	1.000
f_2 = 68.2 cps							
0	-0.700	-0.725	-0.762	-0.795	-0.820	-0.845	-0.858
.25	-.270	-.322	-.390	-.453	-.510	-.545	-.595
.50	.160	.085	-.010	-.115	-.215	-.265	-.345
.75	.595	.492	.370	.240	.110	.050	-.050
1.00	1.000	.872	.720	.562	.400	.310	.200

(d) Model 12D

$\frac{x}{c}$	Normalized deflection at y/l =						
	0	0.15	0.35	0.55	0.75	0.85	1.00
f_1 = 24.3 cps							
0	0.063	0.179	0.353	0.538	0.731	0.833	0.980
.25	.143	.253	.416	.586	.765	.851	.985
.50	.220	.320	.470	.622	.785	.866	.990
.75	.290	.385	.516	.658	.806	.882	.995
1.00	.358	.445	.568	.695	.830	.898	1.000
f_2 = 73.2 cps							
0	-0.555	-0.574	-0.600	-0.632	-0.664	-0.680	-0.710
.25	-.238	-.277	-.330	-.388	-.446	-.475	-.522
.50	.140	.072	-.018	-.110	-.205	-.255	-.332
.75	.560	.462	.332	.200	.060	-.013	-.124
1.00	1.000	.865	.690	.513	.333	.240	.103

TABLE VI.- REPRESENTATIVE COUPLED MODE SHAPES OF TAPERED MODELS - Continued

(e) Model 6W

$\frac{x}{c}$	Normalized deflection at y/l =						
	0	0.15	0.35	0.55	0.75	0.85	1.00
f_1 = 27.0 cps							
0	0.050	0.180	0.351	0.530	0.703	0.793	0.922
.25	.130	.250	.410	.578	.740	.822	.945
.50	.193	.305	.458	.620	.773	.852	.965
.75	.260	.368	.508	.657	.798	.872	.982
1.00	.320	.418	.550	.685	.822	.895	1.000
f_2 = 80.5 cps							
0	-0.532	-0.548	-0.566	-0.582	-0.599	-0.608	-0.620
.25	-.205	-.249	-.295	-.348	-.397	-.423	-.460
.50	.169	.099	.010	-.083	-.169	-.219	-.287
.75	.570	.464	.337	.194	.062	-.010	-.110
1.00	1.000	.857	.680	.490	.305	.211	.072

(f) Model 12W

$\frac{x}{c}$	Normalized deflection at y/l =						
	0	0.15	0.35	0.55	0.75	0.85	1.00
f_1 = 25.1 cps							
0	0.063	0.150	0.300	0.478	0.660	0.758	0.900
.25	.105	.195	.342	.515	.697	.790	.927
.50	.153	.242	.385	.550	.730	.820	.956
.75	.197	.285	.425	.582	.755	.845	.975
1.00	.251	.336	.478	.629	.790	.872	1.000
f_2 = 80.0 cps							
0	-0.470	-0.483	-0.497	-0.508	-0.518	-0.520	-0.522
.25	-.197	-.237	-.285	-.330	-.367	-.381	-.408
.50	.172	.095	0	-.096	-.180	-.217	-.263
.75	.553	.453	.317	.180	.047	-.015	-.095
1.00	1.000	.864	.678	.497	.315	.220	.088

TABLE VI.- REPRESENTATIVE COUPLED MODE SHAPES OF TAPERED MODELS - Concluded

(g) Model 9W

$\frac{x}{c}$	Normalized deflection at y/l =						
	0	0.15	0.35	0.55	0.75	0.85	1.00
f_1 = 26.0 cps							
0	0.047	0.156	0.316	0.500	0.689	0.786	0.938
.25	.093	.196	.353	.530	.718	.812	.957
.50	.163	.257	.405	.571	.748	.836	.976
.75	.230	.319	.454	.610	.778	.860	.990
1.00	.288	.370	.500	.643	.801	.879	1.000
f_2 = 77.2 cps							
0	-0.437	-0.471	-0.504	-0.526	-0.539	-0.543	-0.553
.25	-.186	-.229	-.284	-.339	-.392	-.420	-.455
.50	.147	.084	0	-.093	-.190	-.239	-.314
.75	.549	.461	.333	.196	.049	-.024	-.131
1.00	1.000	.872	.690	.504	.314	.216	.071
f_3 = 265 cps							
0	-0.318	-0.407	-0.477	-0.450	-0.232	0	0.371
.25	-.202	-.311	-.381	-.331	-.066	.166	.504
.50	-.126	-.213	-.268	-.195	.116	.328	.639
.75	-.086	-.159	-.199	-.096	.292	.497	.802
1.00	-.093	-.174	-.174	.066	.484	.692	1.000

TABLE VII.- TEST RESULTS FOR SQUARE MODELS

[Pitch axis at 35 percent chord; panel center of gravity at 53.5 percent chord and 50.0 percent span to within 1/2 percent]

Model	f_1, cps	f_2, cps	$f_{f,exp}$, cps	M	ρ, slugs/cu ft	a, ft/sec	q, lb/sq ft	μ	R_{exp}	Test medium and reflection plane (a)	Uncoupled-mode analysis		Coupled-mode analysis	
											R_{th}	$f_{f,th}$, cps	R_{th}	$f_{f,th}$, cps
0- 9-33-2	12.2	42.3	17.0	1.00	4.78×10^{-4}	508	62.8	396	1.73	F				
			17.4	1.07	4.17	505	62.2	454	1.86					
0- 9-47-4	20.2	66.2	24.5	.97	13.08	512	165.0	144	1.62					
			27.0	1.01	11.06	515	152	170	1.75					
			26.0	1.07	9.56	516	148	197	1.88					
			26.0	1.14	8.37	516	147	225	2.01					
0- 9-47-3	20.2	66.8	28.5	1.17	9.50	512	172	199	2.11					
0- 9-65-3	32.5	103.0	58	1.30	6.12	992	509	311	1.92	3,A	0.94	97.7	----	----
0- 9-65-2	31.5	100.8	60	1.64	6.39	930	742	299	1.96		1.11	96.9	----	----
0- 9-47-5	20.4	67.0	40	2.00	3.05	852	442	623	2.05		1.29	59.0	1.25	44.4
0- 9-65-4	32.0	103.4	65	2.00	7.99	857	1,172	235	1.94		1.29	96.3	1.33	66.3
0- 9-65-1	31.4	102.4	65	2.55	7.55	762	1,424	254	2.24		1.55	94.5	1.74	68.2
0- 9-47-1	20.2	66.2	40	3.00	3.08	700	680	616	2.46		1.77	58.3	1.94	45.4
0- 9-33-1	12.1	41.0	22	3.98	1.13	556	276	1,672	3.14		2.35	34.3	2.51	27.6
0- 9-47-3	20.2	66.1	38	3.98	2.65	594	738	696	3.07		2.23	57.4	2.59	46.1
0- 9-33-3	11.3	41.7	20	6.86	.645	509	392	2,930	4.64	1,A	3.53	32.9	4.31	28.4
0- 9-33-6	11.9	42.9	20	6.86	.584	530	384	3,225	4.80		3.53	32.9	4.29	29.2
0- 9-33-2	11.8	42.4	22	6.83	.242	811	372	7,820	4.83		3.65	32.7	4.52	29.0
0- 9-47-2	20.5	68.0	37	6.83	.565	867	989	3,345	4.74	2,H	3.65	55.6	4.60	47.8
0- 9-65-5	30.9	101.0	55	6.83	1.29	850	2,173	1,482	4.78	2,H	3.65	90.2		
0-14-65-5	31.1	100.2	52	1.30	5.03	989	416	374	2.05	3,A	1.05	95.8	----	----
0-14-65-3	32.6	105.6	65	1.64	6.41	930	746	294	2.04		1.25	94.9	1.01	64.4
0-14-65-5	31.4	100.8	62	2.00	7.04	867	1,060	267	1.99		1.47	94.1	1.34	65.4
0-14-47-1	20.4	70.4	40	3.00	3.00	704	670	617	2.60		2.06	56.9	1.91	48.3
0-14-47-2	18.4	66.8	38	3.98	2.27	593	632	800	3.33		2.61	56.1	2.50	45.9
0-14-65-1	31.6	105.0	62	6.83	1.20	811	1,030	1,373	5.37	2,H	4.35	87.2	4.61	72.0
0-20-65-6	33.6	111.6	67	1.30	4.35	987	357	426	2.44	3,A	1.16	94.6	1.29	74.7
0-20-65-4	33.6	109.6	63	1.64	4.95	927	570	370	2.37		1.40	93.7	1.60	74.1
0-20-65-6	33.4	111.0	67	2.00	5.92	861	878	313	2.39		1.64	92.8	2.00	75.7
0-20-47-3	20.0	69.4	38	3.00	2.42	698	532	760	2.87		2.32	55.8	2.84	48.2
0-20-47-3	20.0	69.4	36	3.98	2.23	592	619	824	3.52		2.96	54.9	3.74	48.7
0-20-65-4	33.2	111.6	55	6.83	.764	906	1,462	2,395	6.30	2,H	4.76	85.3	6.59	75.0
0-20-47-1	20.0	70.1	35	6.83	.354	844	588	5,070	6.19	2,H	4.76	52.5	6.28	48.7
1-11-47-5	19.3	66.6	38.0	.94	14.47	503	163	132	1.59	F				
			25.5	.95	12.75	508	151	149	1.67					
			24.4	1.01	11.17	508	149	170	1.79					
			25.4	1.11	9.34	506	150	203	1.99					
			28.0	1.17	9.89	515	183	190	1.86					
1-11-65-3	32.2	101.6	58	1.30	6.89	991	574	270	1.76	3,A				
1-11-65-1	32.0	102.2	61	1.64	7.74	932	904	242	1.78					
1-11-47-4	20.6	69.3	40	2.00	4.28	858	630	449	1.80					
1-11-47-6	19.5	65.4	39	2.00	3.75	858	552	510	1.80					
1-11-65-2	33.0	104.0	64	2.55	8.14	764	1,547	234	2.17					

[a]Numbers refer to reflection plane used (see fig. 3); no number indicates boundary-layer fillet was used; letters refer to test medium: A - air, F - Freon-12, H - helium.

TABLE VII.- TEST RESULTS FOR SQUARE MODELS - Concluded

Model	f_1, cps	f_2, cps	$f_{f,exp}$, cps	M	ρ, slugs/cu ft	a, ft/sec	q, lb/sq ft	μ	R_{exp}	Test medium and reflection plane (a)	Uncoupled-mode analysis		Coupled-mode analysis	
											R_{th}	$f_{f,th}$, cps	R_{th}	$f_{f,th}$, cps
1-11-47-1	20.5	68.4	41	3.00	3.53×10^{-4}	699	777	526	2.34	3,A				
1-11-33-5	12.1	41.0	22	3.98	1.128	556	276	1,672	2.83	↓				
1-11-47-5	19.4	65.6	38	3.98	3.205	595	900	582	2.78					
1-11-33-1	11.8	43.4	23	6.83	.343	804	516	5,530	4.20	1,H				
1-11-33-4	11.7	43.2	22	6.86	.904	510	549	2,053	4.01	1,A				
1-11-47-2	19.9	67.6	40	6.83	.645	848	1,080	2,900	4.40	2,H				
1-11-47-3	20.4	67.4	36	6.83	.594	868	1,045	3,115	4.53	2,H				
3-14-47-2	20.2	70.0	33.4	.83	23.06	508	210	80	1.28	F				
			30.5	.87	20.26	510	203	91	1.37					
			25.5	.90	17.63	510	189	104	1.46					
			26.0	.92	15.61	512	176	118	1.55					
			26.4	.93	13.87	514	160	133	1.64					
			26.6	.96	12.63	514	154	146	1.72					
			25.2	.98	11.38	514	148	161	1.81					
			31.0	1.14	13.13	506	224	140	1.71	↓				
3-14-65-2	32.8	109.4	62	1.30	9.40	996	787	198	1.61	3,A				
3-14-47-2	20.6	69.6	41	1.30	4.00	989	330	460	1.58					
3-14-65-1	32.5	107.2	68	1.64	10.06	935	1,184	184	1.63					
3-14-47-1	20.9	72.8	45	2.00	5.40	860	798	343	1.64					
3-14-65-5	31.9	108.0	71	2.00	12.12	860	1,795	159	1.66					
3-14-65-3	33.2	112.2	70	2.55	11.81	760	2,217	159	1.95					
3-14-47-4	20.8	72.6	44	3.00	5.25	703	1,170	360	2.05					
3-14-33-3	12.4	44.2	26	3.98	1.893	588	517	974	2.48	↓				
3-14-33-1	12.0	44.0	22	6.83	.386	819	607	4,782	3.88	2,H				
3-14-47-1	20.5	72.4	36	6.83	.903	885	1,646	2,050	3.87	2,H				
6-20-47-1	20.8	74.4	44.4	.71	38.26	502	249	47	1.06	F				
			39.8	.78	31.04	502	245	58	1.18					
			32.0	.86	23.93	502	228	75	1.34					
			30.2	.89	21.25	501	215	85	1.43					
			29.5	.90	19.40	501	202	93	1.49					
			28.0	.91	18.15	502	195	99	1.54					
			----	1.03	22.65	499	303	79	1.37					
6-20-47-2	20.3	72.0	35.0	1.06	21.00	497	298	87	1.41	↓				
6-20-65-3	34.1	117.5	67	1.30	9.36	987	769	193	1.73	3,A				
6-20-65-1	32.6	115.0	68	1.30	9.51	990	788	145	1.70					
6-20-47-2	19.8	70.0	39	1.30	3.41	989	282	534	1.71					
6-20-65-1	32.6	116.0	(b)	1.64	15.26	920	1,728	121	1.45					
6-20-47-1	20.8	73.7	(b)	2.00	5.00	859	732	359	1.69					
6-20-65-2	32.4	117.6	(b)	2.55	11.82	760	2,218	159	2.05					
6-20-65-6	34.0	115.0	(b)	2.55	12.15	752	2,230	152	1.97					
6-20-47-3	20.4	72.6	(b)	3.00	4.23	702	939	434	2.25					
6-12-47-2	20.7	70.6	(b)	3.00	4.63	710	1,052	382	2.03					
6-20-33-1	12.4	44.2	(b)	3.98	1.316 to 1.505	582 to 582	353 to 403	1,212 to 1,387	2.76 to 2.96	↓				
6-20-47-2	20.6	74.0	(b)	6.83	.681	870	1,200	2,673	4.60	2,A				
6-20-47-2	20.5	73.6	(b)	6.83	.670	870	1,180	2,720	4.61	2,A				

[a] Numbers refer to reflection plane used (see fig. 3); no number indicates boundary-layer fillet was used; letters refer to test medium: A - air, F - Freon-12, H - helium.

[b] Model diverged.

TABLE VIII.- TEST RESULTS FOR TAPERED MODELS

Model configuration	Natural frequencies, cps			$f_{f,exp}$, cps	M	ρ, slugs/cu ft	a, ft/sec	q, lb/sq ft	μ	R_{exp}	Uncoupled-mode analysis		Coupled-mode analysis	
	f_1	f_2	f_3								R_{th}	$f_{f,th}$, cps	R_{th}	$f_{t,th}$, cps
3D-2	26	79	269	45	0.71	30.96×10^{-4}	510	203	50.0	1.035				
				45	.76	25.63	511	198	60.3	1.132				
				43	.85	18.83	516	185	82.1	1.310				
				38	.92	14.92	518	169	106.4	1.510				
				38	.94	12.88	518	157	120.0	1.603				
				36	.98	11.60	510	147	133.2	1.687				
				34	1.02	11.20	512	156	138.0	1.714				
				34	1.03	11.11	518	162	139.0	1.697				
				N.F.	1.08	10.66	508	164	145.0	1.718				
				38	1.16	11.70	507	207	132.0	1.677				
3D-1	28	86	273	51	1.30	4.38	995	367	353	1.540	1.112	67.5	1.515	62.7
	28	86	278	58	1.64	5.16	930	599	299	1.517	1.304	67.4	1.730	62.1
	28	89	275	58	2.00	6.05	871	918	255	1.550	1.485	67.2	1.938	63.8
	28	87	280	55	2.55	5.93	784	1,184	261	1.695	1.716	66.8	2.370	62.3
	28	86	276	60	3.00	5.55	718	1,287	270	1.893	1.897	66.3	2.600	59.7
	27	85	276	54	3.00	5.79	719	1,350	266	1.827	1.893	66.4	2.455	61.0
3D-3	18	56	252	35	3.00	2.48	698	545	622	1.897	1.905	44.1	2.470	40.0
3D-3	18	57	250	34	3.98	2.67	602	768	578	2.160	2.196	41.4	2.945	40.2
6D-2	21	63	254	38	.68	29.73	497	170	63.4	.947				
				38	.73	25.20	498	168	77.0	1.044				
				37	.78	21.65	502	167	87.0	1.098				
				34	.83	18.66	500	162	101	1.190				
				32	.89	15.68	502	158	120	1.292				
				30	.94	12.91	500	144	146	1.430				
				29	.98	11.32	502	138	166	1.514				
				27	1.03	9.69	502	131	194	1.642				
				27	1.07	9.24	501	136	204	1.687				
				28	1.13	8.83	506	150	213	1.708				
6D-1	24	73	267	50	1.30	3.14	990	260	599	1.716	1.182	59.2	1.482	53.2
	25	74	268	46	1.64	3.99	928	462	472	1.645	1.367	58.8	1.720	53.7
	24	76	268	47	2.00	4.60	864	697	409	1.687	1.546	58.4	1.935	54.3
	25	77	268	50	2.55	4.59	774	894	411	1.915	1.813	57.9	2.285	54.7
	25	73	270	50	3.00	4.09	711	929	460	2.088	2.023	57.5	2.590	52.7
	24	75	268	47	3.00	4.43	714	1,017	425	2.050	2.033	57.7	-----	----
6D-3	17	49	248	30	3.98	1.83	590	505	1,028	2.532	2.527	37.6	3.070	35.2
6W-2	26	73	261	46	.70	23.12	502	145	64.0	1.103				
				44	.76	19.95	501	145	74.1	1.186				
				40	.81	16.47	502	139	89.8	1.307				
				39	.86	13.26	506	129	111.5	1.444				
				36	.92	10.65	504	115	138.8	1.618				
				33	.97	8.42	512	105	175.5	1.792				
				33	1.02	7.08	511	98	209.0	1.955				
				33	1.06	6.49	506	95	228.0	2.065				
				33	1.11	7.24	506	116	204.0	1.954				
				33	1.15	7.39	512	130	200.0	1.913				
6W-1	29	87	270	60	1.30	4.43	993	369	334	1.518	1.100	70.0	1.114	73.1
	26	86	270	61	1.64	5.17	928	599	286	1.487	1.252	70.9	1.245	71.8
	28	89	270	59	2.00	5.57	866	836	265	1.584	1.384	70.0	1.390	74.2
	28	88	270	60	2.55	6.03	780	1,190	245	1.670	1.574	70.0	1.572	73.7
	28	88	268	54	3.00	5.82	718	1,353	254	1.850	1.723	70.4	1.740	73.6
6W-3	19	60	252	37	3.98	2.90	600	833	308	2.143	2.200	46.5	2.02	50.7
9W-2	25	69	256	43	.68	26.98	504	163	58.5	.992				
				40	.80	19.03	509	159	83.0	1.172				
				37	.86	15.77	511	155	100.0	1.280				
				37	.91	14.09	508	152	112.0	1.352				
				36	.94	12.45	509	146	126.7	1.447				
				33	.98	10.90	508	139	144.7	1.548				
				30	1.01	10.19	506	136	154.8	1.608				
				30	1.04	9.41	507	133	167.7	1.667				
				30	1.07	8.45	506	126	187.0	1.767				
				32	1.09	7.77	510	121	203.0	1.822				
				32	1.12	8.06	512	135	196.0	1.792				
				33	1.13	8.61	511	147	183.2	1.732				

TABLE VIII.- TEST RESULTS FOR TAPERED MODELS - Concluded

Model configuration	Natural frequencies, cps			$f_{f,exp}$, cps	M	ρ, slugs/cu ft	a, ft/sec	q, lb/sq ft	μ	R_{exp}	Uncoupled-mode analysis		Coupled-mode analysis	
	f_1	f_2	f_3								R_{th}	$f_{f,th}$, cps	R_{th}	$f_{f,th}$, cps
9W-1	26	81	268	60	1.30	4.70×10^{-4}	992	391	326	1.397	1.132	66.3	0.782	88.6
	25	82	262	58	1.64	6.06	932	706	259	1.350	1.309	66.9	.908	89.1
	27	85	270	56	2.00	6.62	871	1,003	238	1.424	1.427	65.5	1.012	92.2
	28	82	270	57	2.55	6.60	785	1,322	239	1.530	1.637	65.4	1.162	89.2
	27	82	264	56	3.00	6.57	721	1,558	240	1.672	1.816	66.1	1.280	89.0
	26	80	270	55	3.00	6.64	724	1,563	237	1.615	1.812	66.0	1.273	87.2
9W-3	18	53	250	35	3.98	3.14	606	910	502	1.857	2.158	43.9	1.445	59.5
9D-2	21	62	248	37	.71	26.79	496	171	71.2	.997				
				36	.77	23.32	499	172	81.8	1.063				
				32	.86	19.64	498	183	97.2	1.160				
				28	.91	15.63	498	163	122.0	1.300				
				29	.90	16.75	499	173	113.8	1.253				
				29	.92	14.43	498	155	132.2	1.353				
				28	.94	13.15	498	146	145.0	1.416				
				27	1.08	11.10	497	162	172.0	1.548				
				27	1.13	9.89	499	158	193.0	1.632				
				27	1.13	9.65	495	154	198.0	1.665				
				28	1.17	8.58	495	146	222.5	1.766				
9D-1	24	73	263	46	1.30	2.87	988	237	663	1.783	1.192	57.3	1.611	49.2
	25	74	266	46	1.64	3.72	926	428	572	1.720	1.420	56.9	1.915	49.8
	24	74	267	45	2.00	3.99	862	592	478	1.780	1.616	56.4	2.170	49.3
	24	73	263	44	2.55	3.72	770	716	511	2.030	1.906	55.8	2.530	48.4
	24	74	266	42	3.00	3.74	710	848	508	2.230	2.158	55.3	2.87	48.2
	24	73	264	45	3.00	3.56	709	805	534	2.225	2.142	55.3	-----	----
9D-3	16	52	240	27	3.98	1.82	593	510	1,046	2.690	2.870	36.7	3.550	35.9
12D-2	22	65	319	40	.71	27.47	504	181	65.0	.985				
				38	.79	24.98	503	200	71.5	1.036				
				33	.84	22.79	502	205	78.3	1.086				
				30	.88	18.53	503	185	96.3	1.202				
				31	.92	15.52	503	171	115.0	1.313				
				31	.97	13.03	502	159	137.0	1.436				
				31	.99	13.04	500	161	137.0	1.442				
				31	1.04	13.04	506	185	137.0	1.425				
				30	1.06	12.90	504	188	138.3	1.437				
				31	1.09	11.82	503	180	151.0	1.505				
				30	1.12	10.67	504	172	167.2	1.581				
				30	1.18	9.32	502	165	191.5	1.697				
12D-1	26	78	334	40	1.30	2.79	988	230	639	1.893	1.341	60.2	1.580	58.0
	24	79	338	43	1.64	3.50	923	401	509	1.833	1.573	59.6	1.840	57.3
	26	80	336	50	2.00	3.78	862	598	471	1.910	1.810	59.2	2.140	57.6
	27	81	340	46	2.55	3.66	768	701	486	2.21	2.171	58.3	2.580	57.6
	26	79	335	47	3.00	3.31	708	748	538	2.457	2.460	57.8	2.920	55.2
12D-3	17	50	284	25	2.98	1.37	572	355	1,300	2.990	2.963	37.7	3.600	34.4
12W-2	24	69	250	43	.70	24.90	502	156	61.5	1.020				
				40	.78	20.07	501	156	76.2	1.141				
				38	.84	16.58	500	149	923	1.257				
				36	.91	13.82	498	145	110.6	1.382				
				33	.97	11.56	500	138	132.4	1.505				
				32	1.02	10.14	498	133	150.8	1.613				
				30	1.06	8.55	512	128	179.0	1.707				
				31	1.07	8.38	503	122	182.6	1.757				
				30	1.07	7.93	513	122	193.0	1.775				
				30	1.08	8.35	505	126	183.2	1.751				
				31	1.11	8.17	512	133	187.2	1.748				
				42	1.16	9.62	506	170	159.0	1.630				
12W-1	28	86	275	60	1.30	4.70	992	391	326	1.483	1.150	67.8	1.023	84.8
	24	86	260	59	1.64	6.25	930	727	244	1.372	1.310	67.8	1.142	84.5
	24	86	268	58	2.00	6.64	872	1,010	230	1.420	1.460	67.1	1.282	84.5
	27	86	265	57	2.55	6.60	785	1,322	231	1.575	1.660	67.2	1.485	84.5
	27	84	268	58	3.00	6.03	720	1,407	253	1.762	1.857	67.2	1.757	83.5
	26	85	264	55	3.00	6.17	723	1,450	247	1.755	1.817	65.8		
12W-3	18	56	240	37	3.98	2.78	602	798	549	2.065	2.293	44.3	1.963	55.3

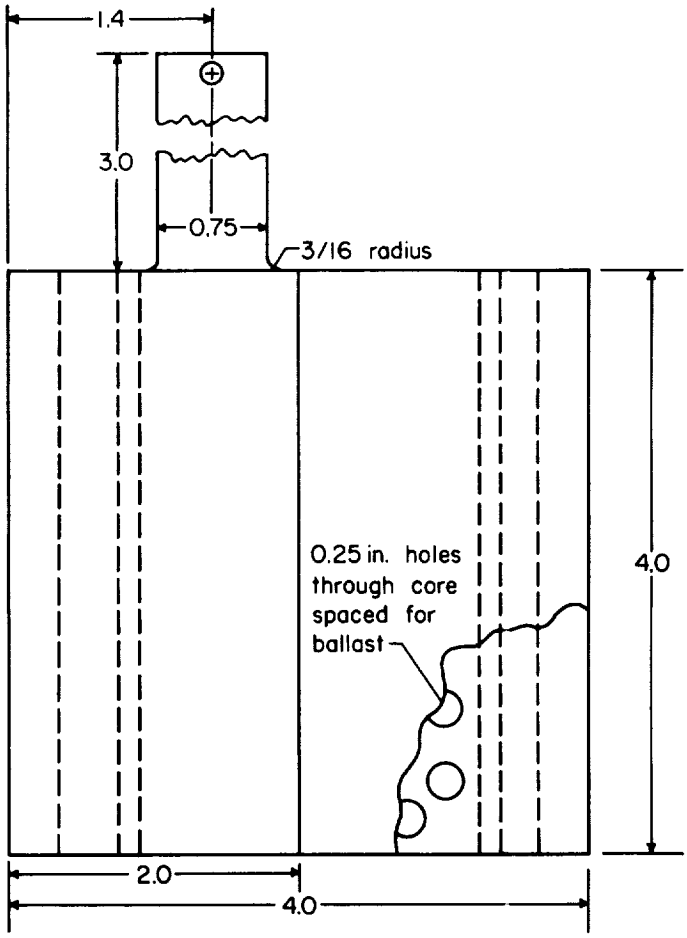

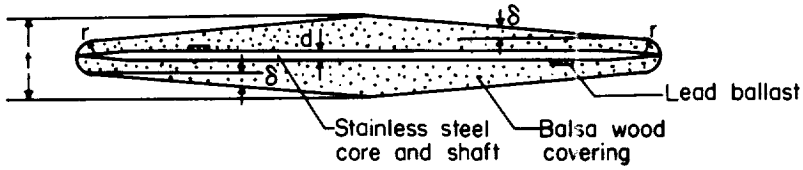

Dimension	Values (see table I)
r	0, 0.04, 0.12, 0.24 in.
d	0.033, 0.047, 0.065 in.
t	0.35, 0.43, 0.56, 0.80 in.
δ	5.0, 8.0, 11.3 deg

Figure 1.- Model geometry and construction of square models. Dimensions are in inches.

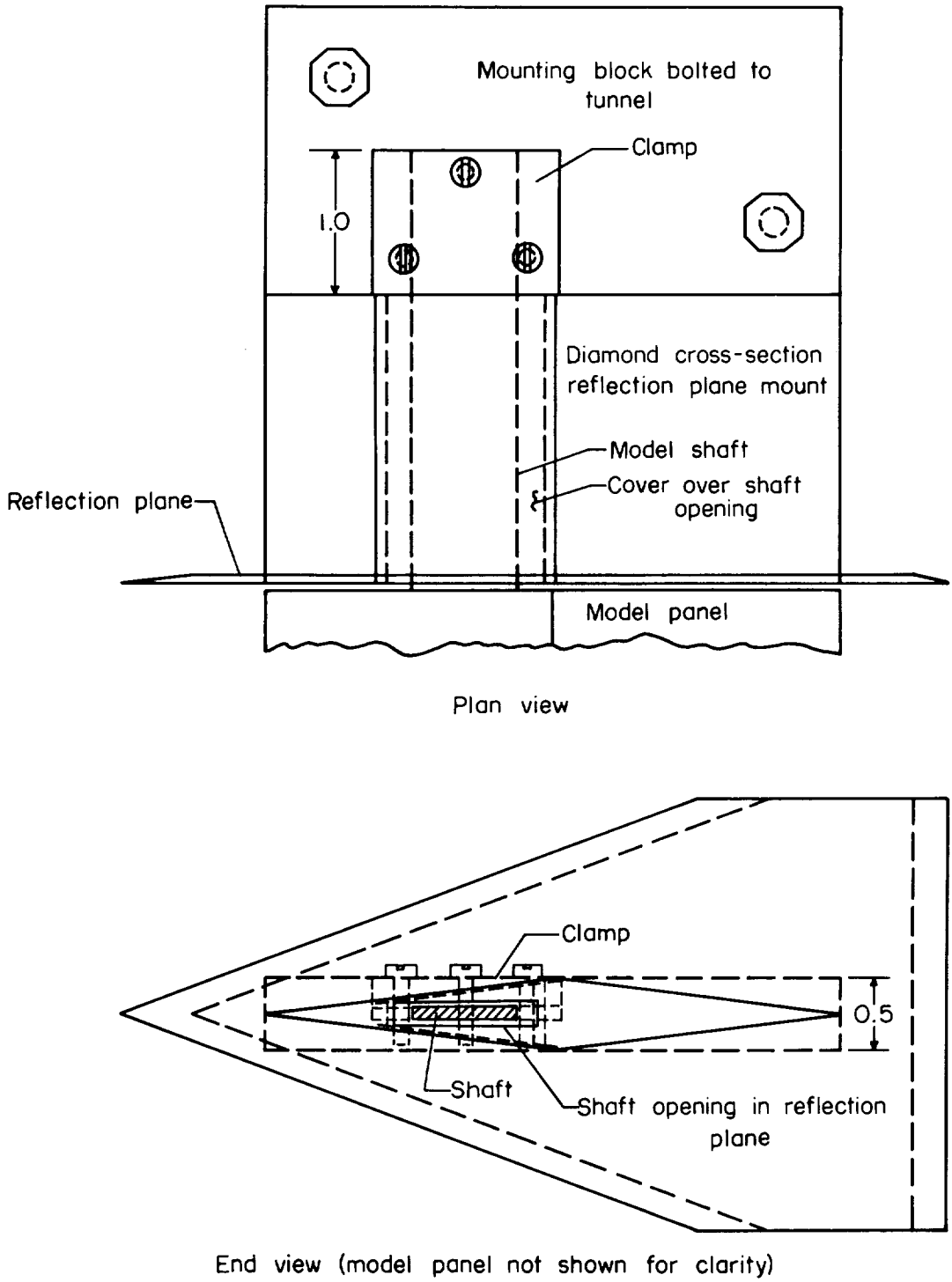

Figure 2.- Square-model mounting system. Dimensions are in inches.

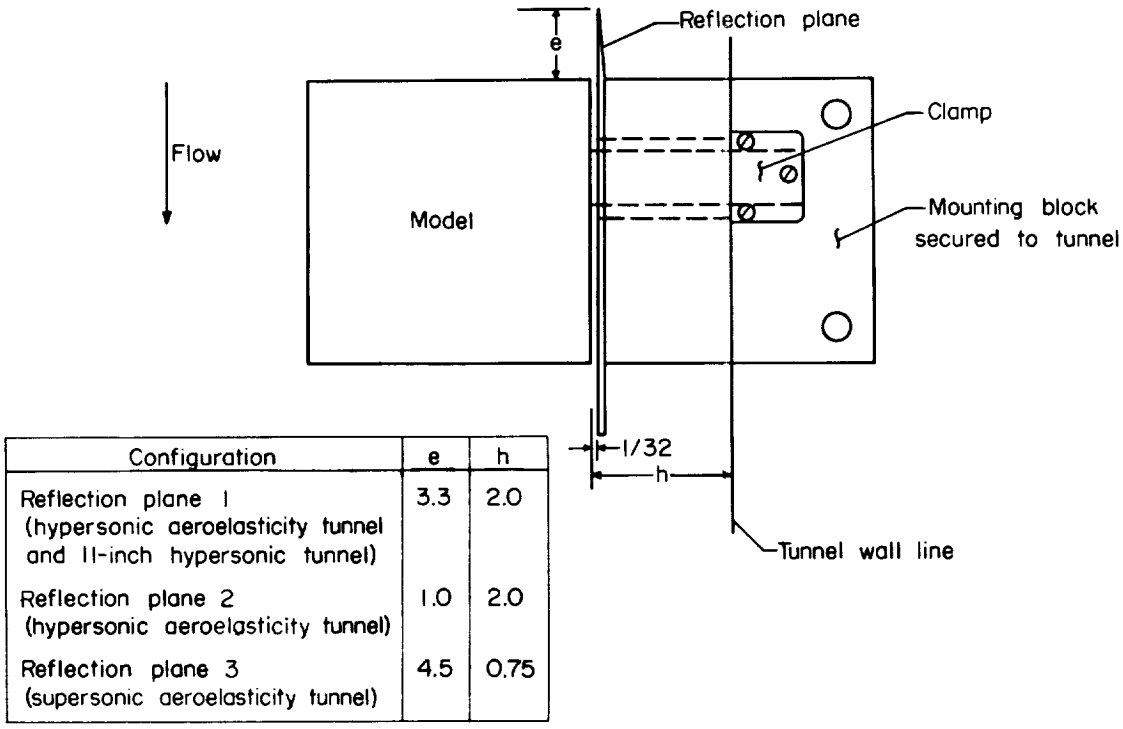

Configuration	e	h
Reflection plane 1 (hypersonic aeroelasticity tunnel and 11-inch hypersonic tunnel)	3.3	2.0
Reflection plane 2 (hypersonic aeroelasticity tunnel)	1.0	2.0
Reflection plane 3 (supersonic aeroelasticity tunnel)	4.5	0.75

(a) Supersonic and hypersonic reflection-plane configurations.

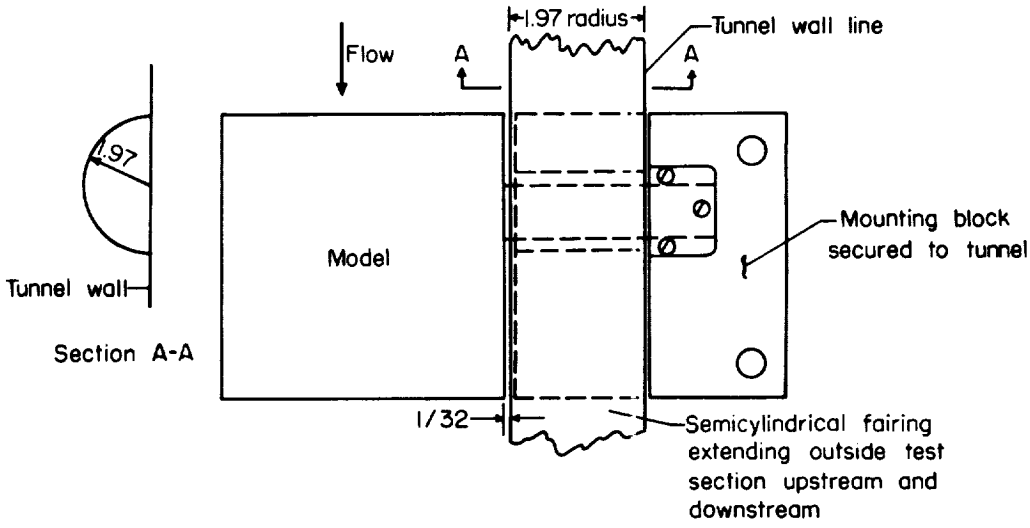

(b) Transonic boundary-layer semicircular fairing (solid).

Figure 3.- Methods used in the various tunnels to reduce tunnel boundary-layer effects on square models. All dimensions are in inches.

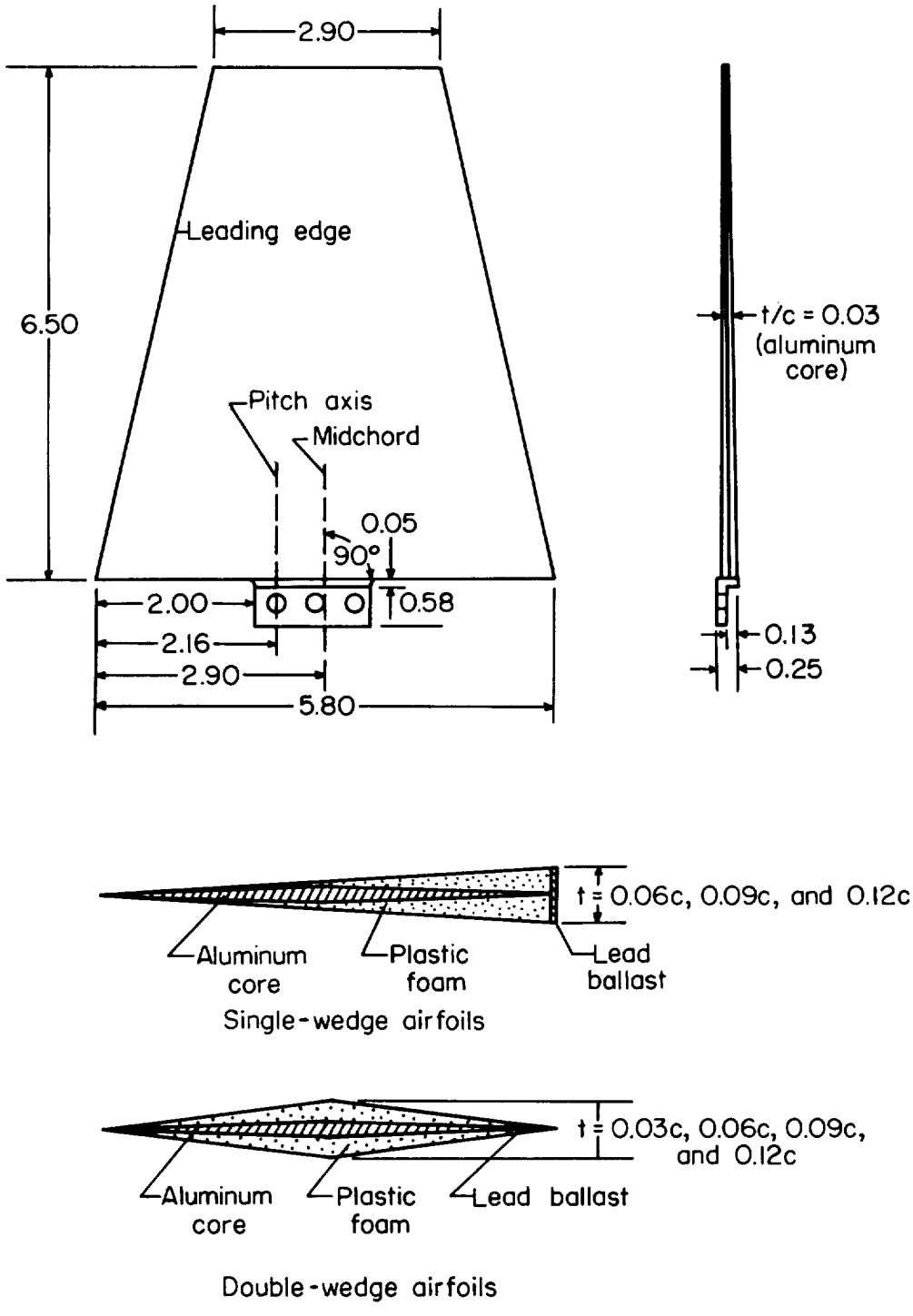

Figure 4.- Geometry and construction of tapered models. All dimensions are in inches.

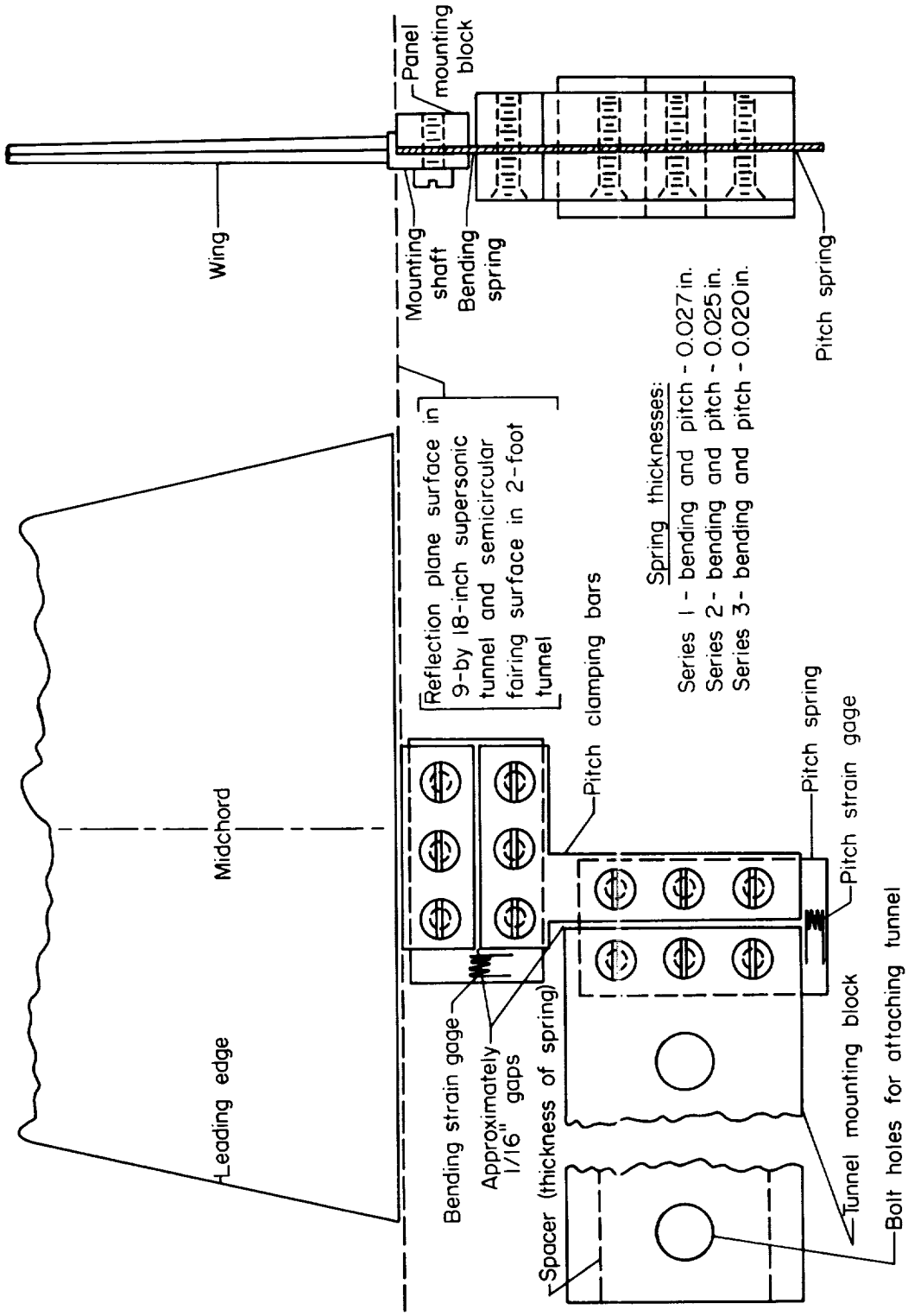

Figure 5.- Tapered-model mounting system.

L-1626

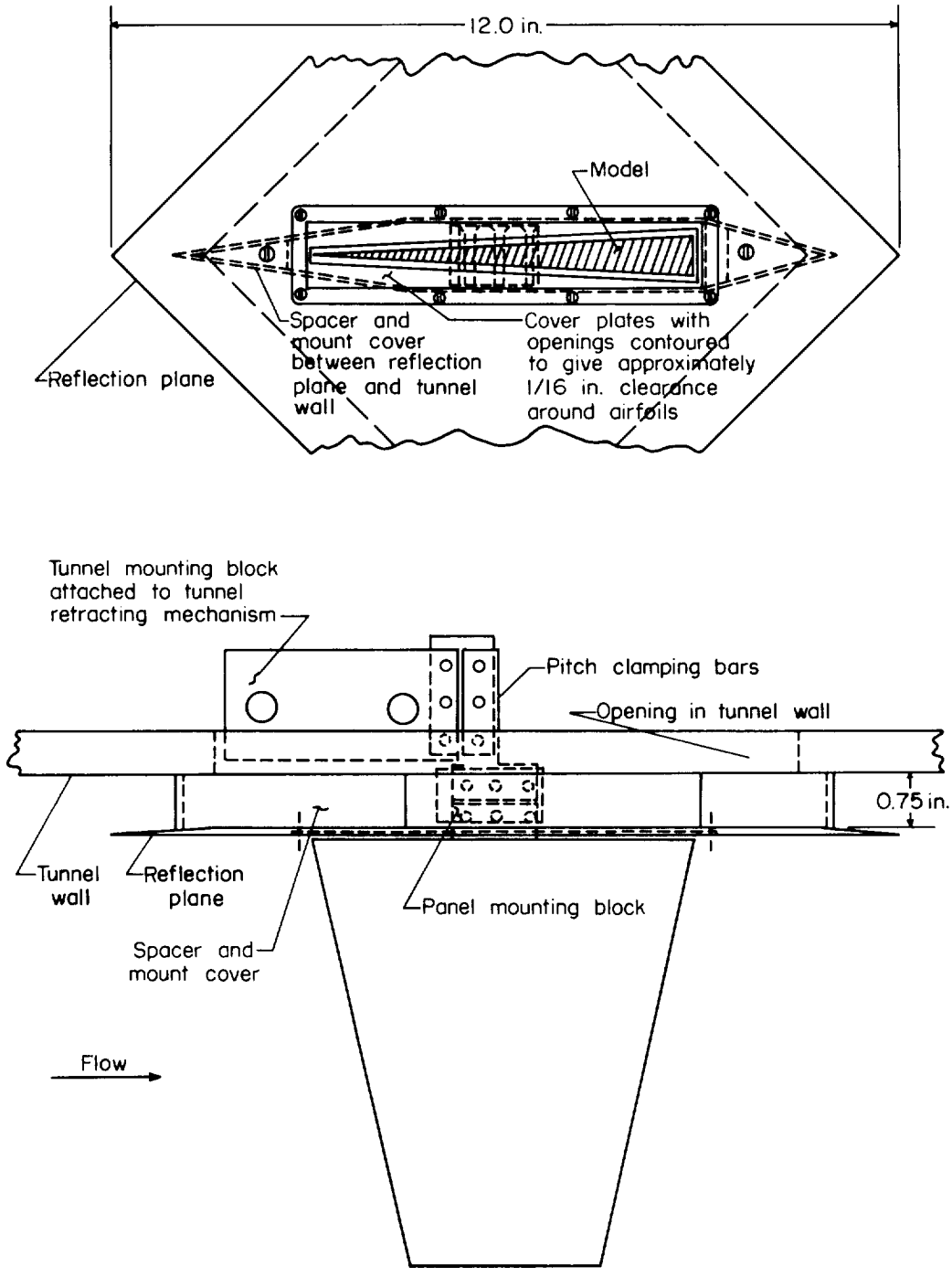

(a) Langley 9- by 18-inch supersonic aeroelasticity tunnel.

Figure 6.- Method of mounting tapered models in tunnels.

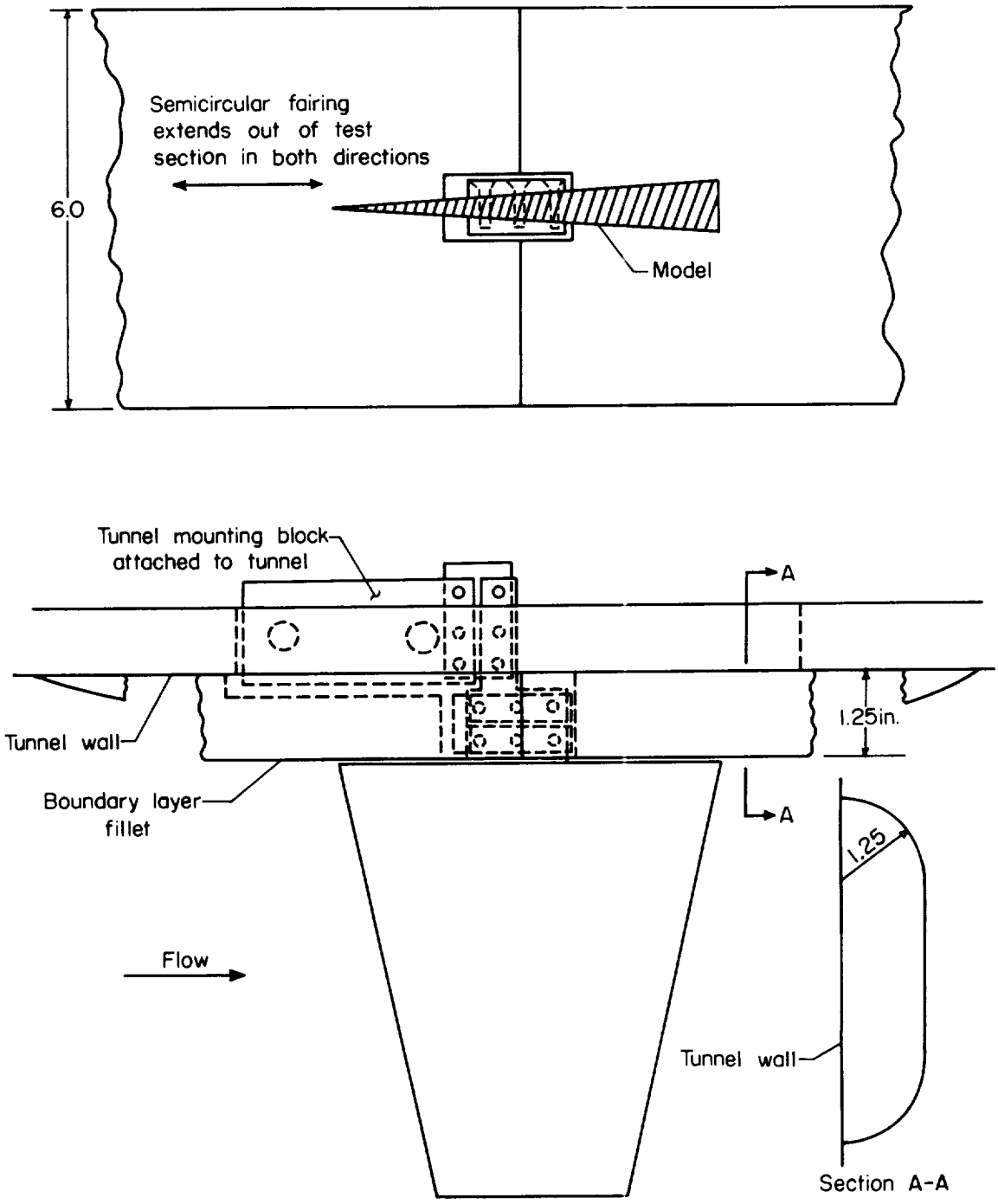

(b) Langley 2-foot transonic aeroelasticity tunnel.

Figure 6.- Concluded.

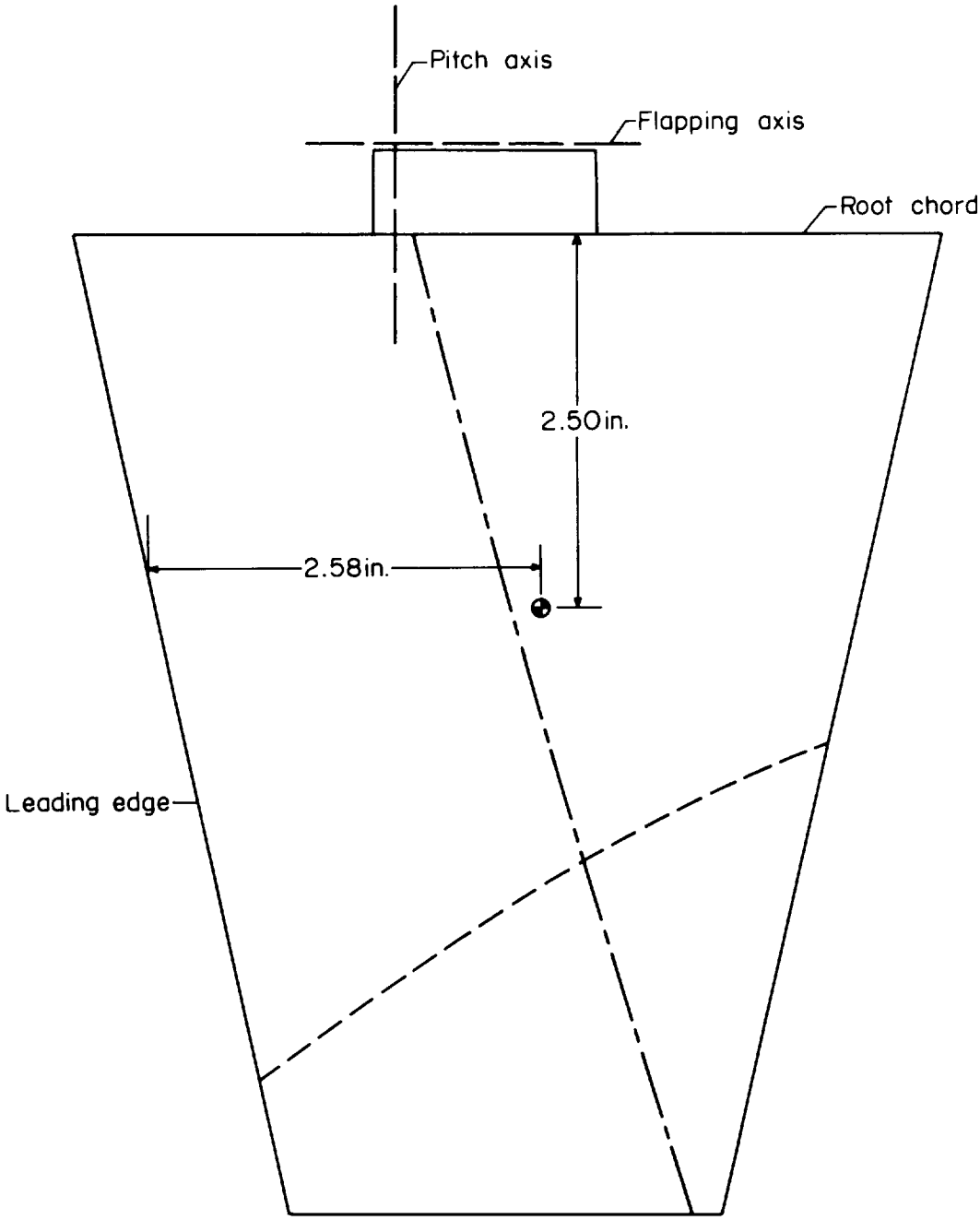

● Panel (including mounting shaft) c.g.
——— f_2 typical node line
— — — f_3 typical node line

Figure 7.- Typical node lines for tapered models.

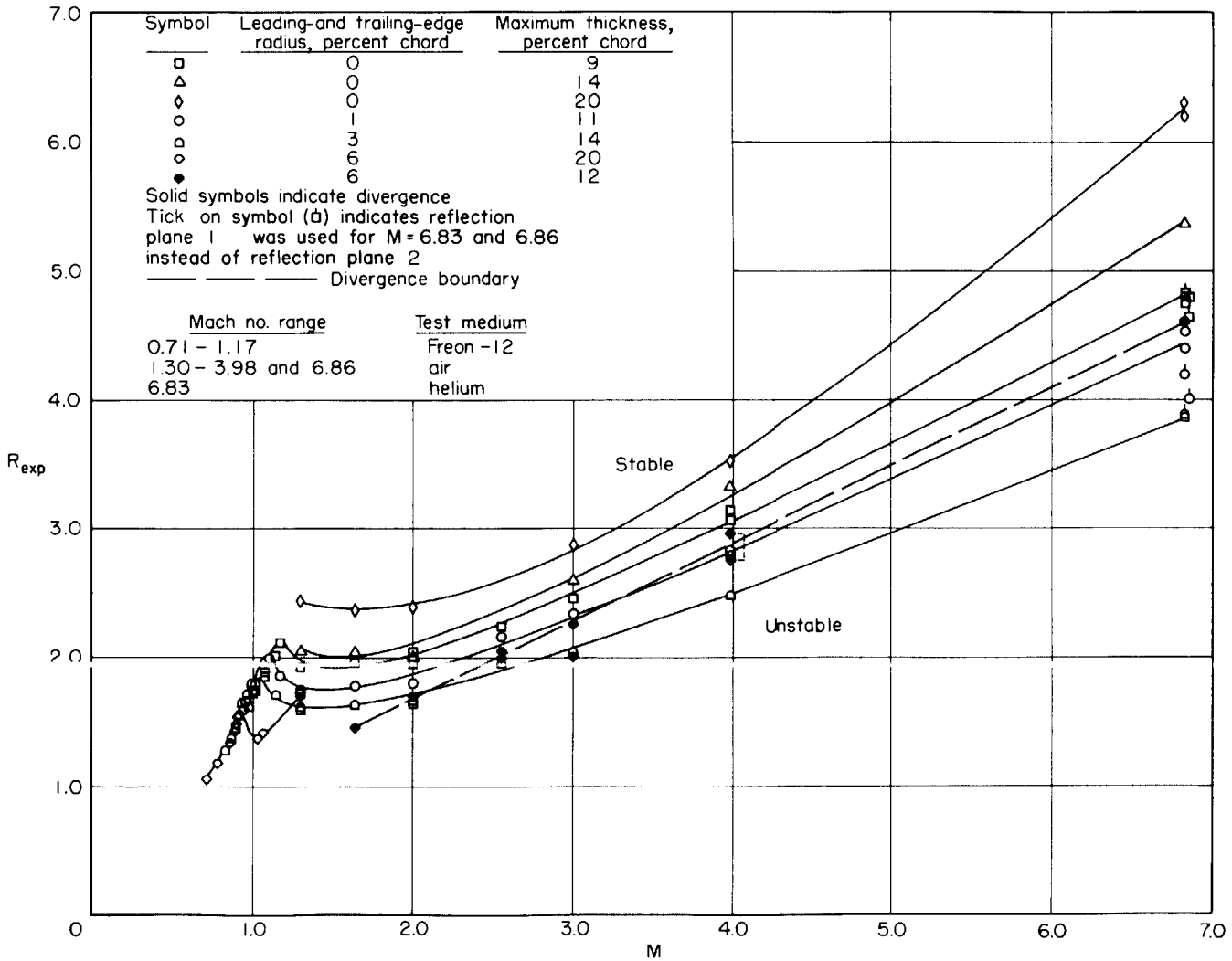

Figure 8.- Experimental variation of stiffness-altitude parameter with Mach number for square models.

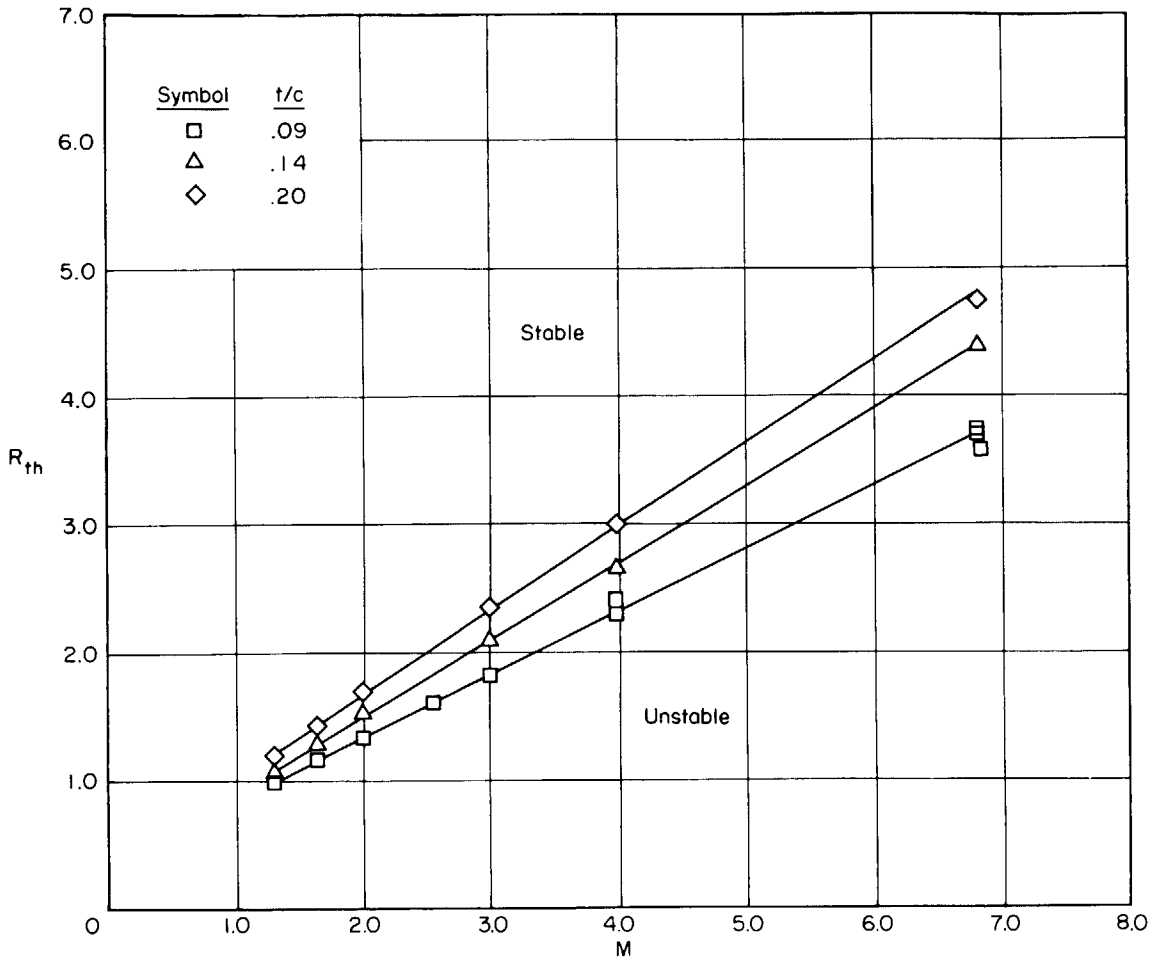

(a) Uncoupled-mode analysis.

Figure 9.- Theoretical variation of stiffness-altitude parameter with Mach number for square models with sharp leading and trailing edges.

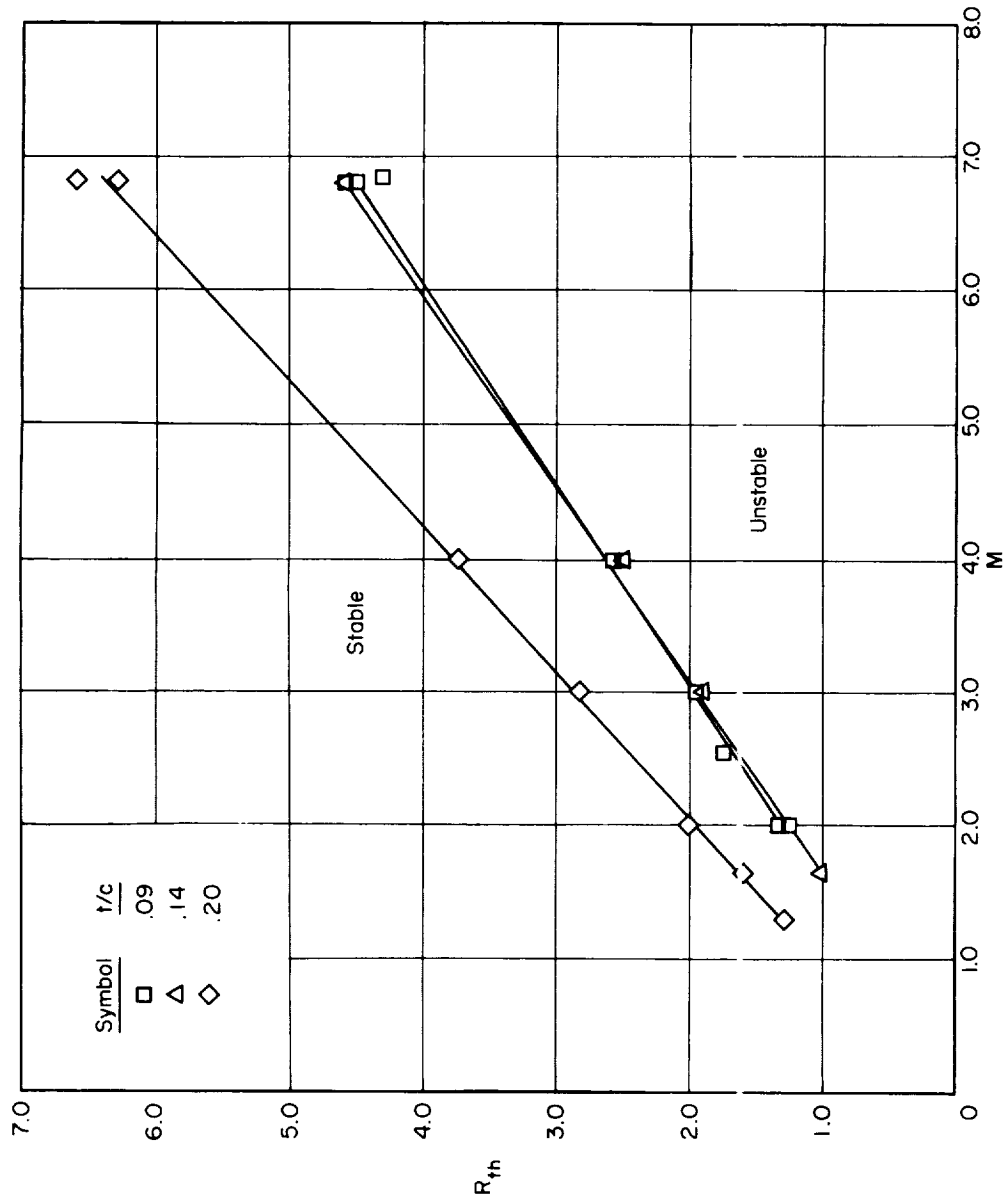

(b) Coupled-mode analysis.

Figure 9.- Concluded.

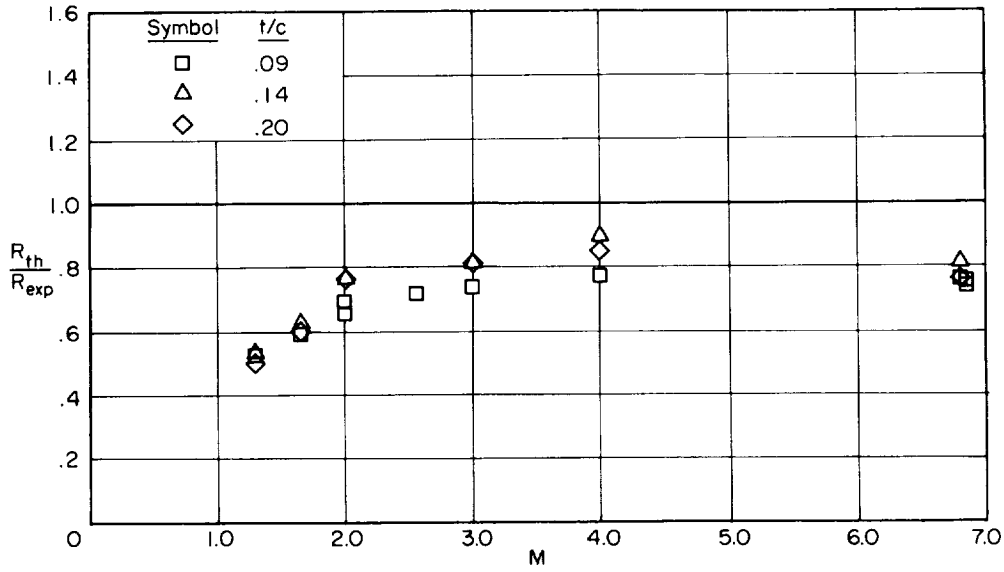

(a) Uncoupled-mode analysis.

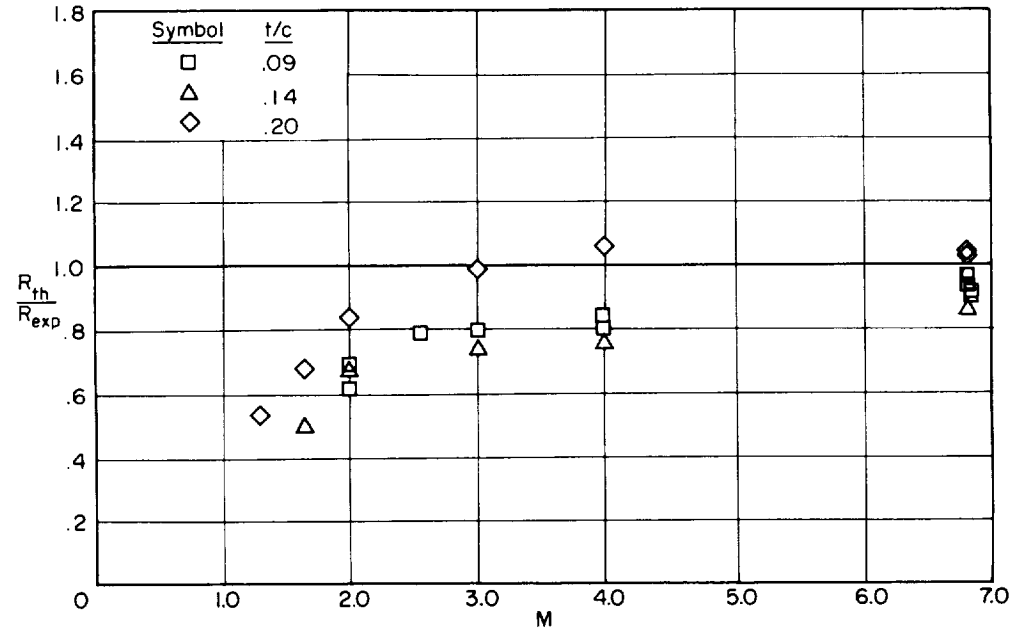

(b) Coupled-mode analysis.

Figure 10.- Comparison of experimental and theoretical stiffness-altitude parameters for square models with sharp leading and trailing edges.

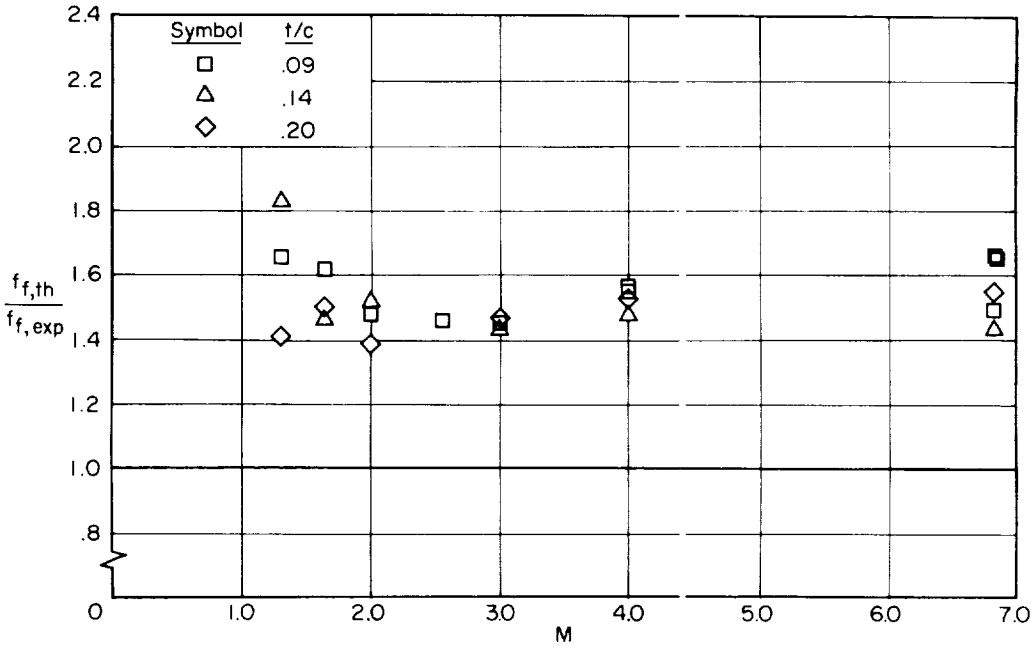

(a) Uncoupled-mode analysis.

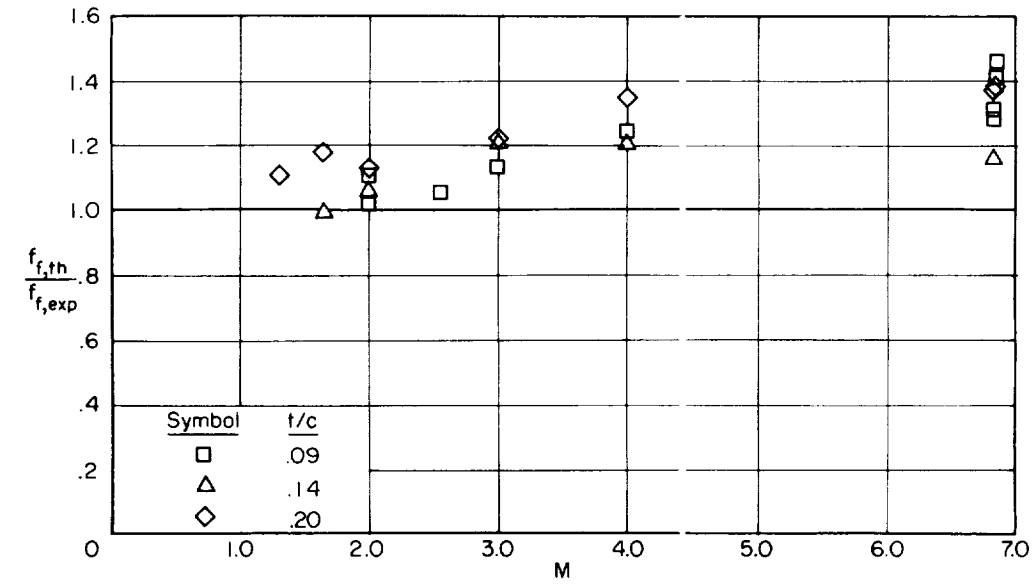

(b) Coupled-mode analysis.

Figure 11.- Comparison of experimental and theoretical flutter frequencies for square models.

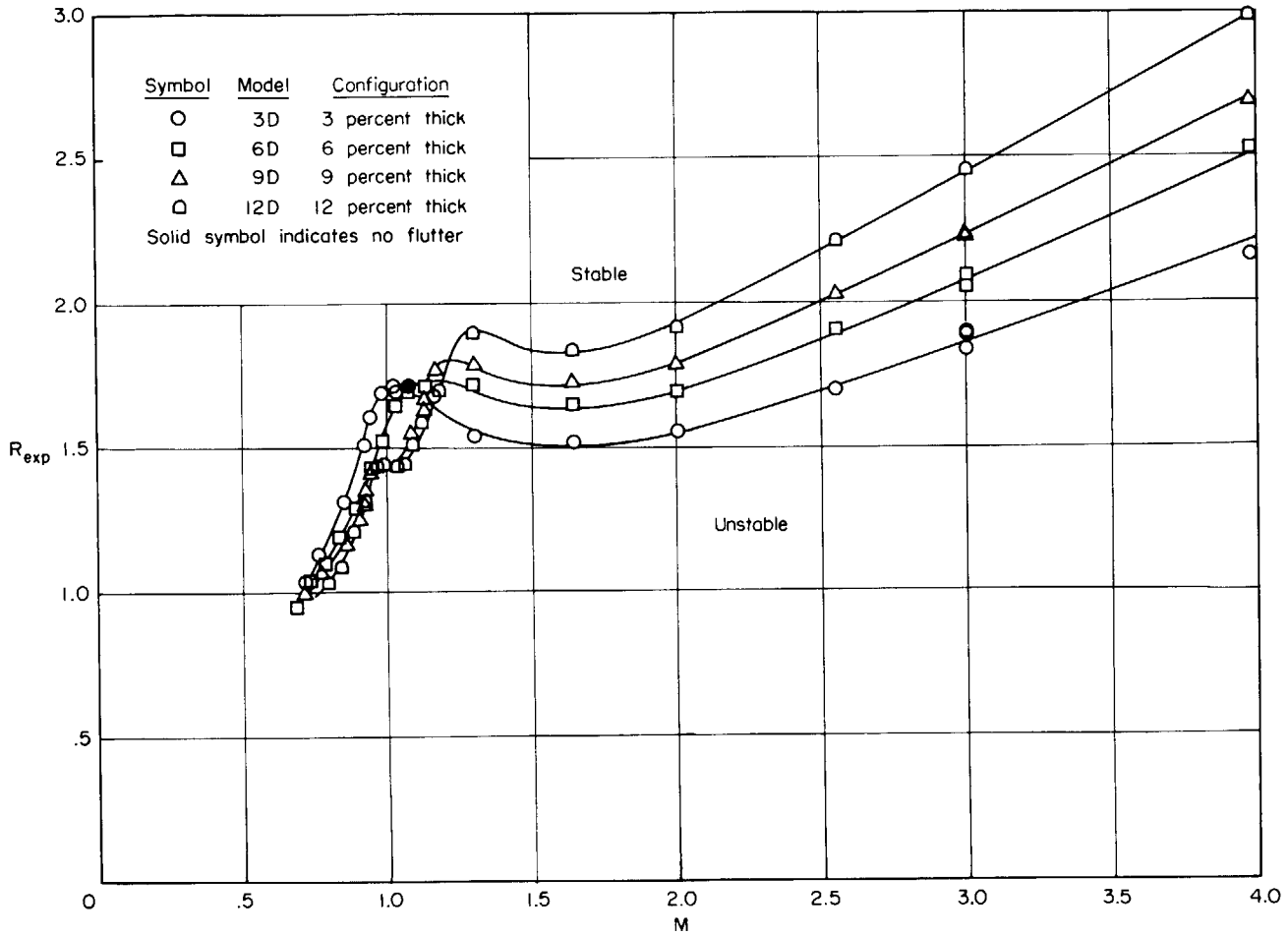

(a) Double-wedge airfoil.

Figure 12.- Experimental variation of stiffness-altitude parameter with Mach number for tapered models.

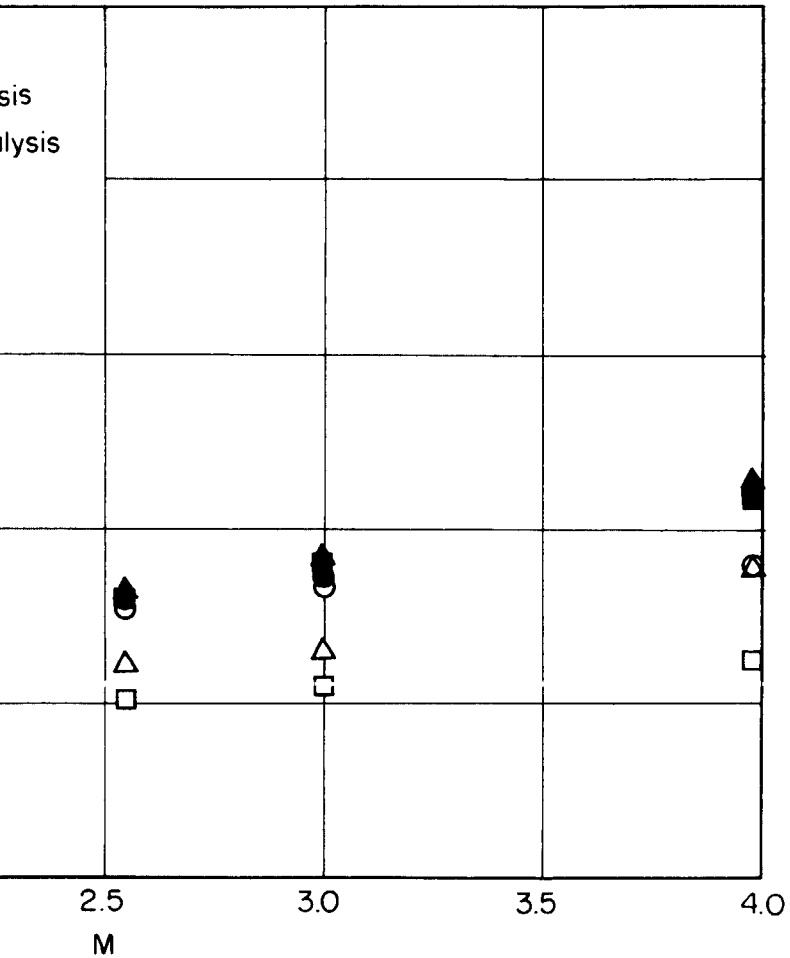

gle-wedge airfoil.

13.- Concluded.

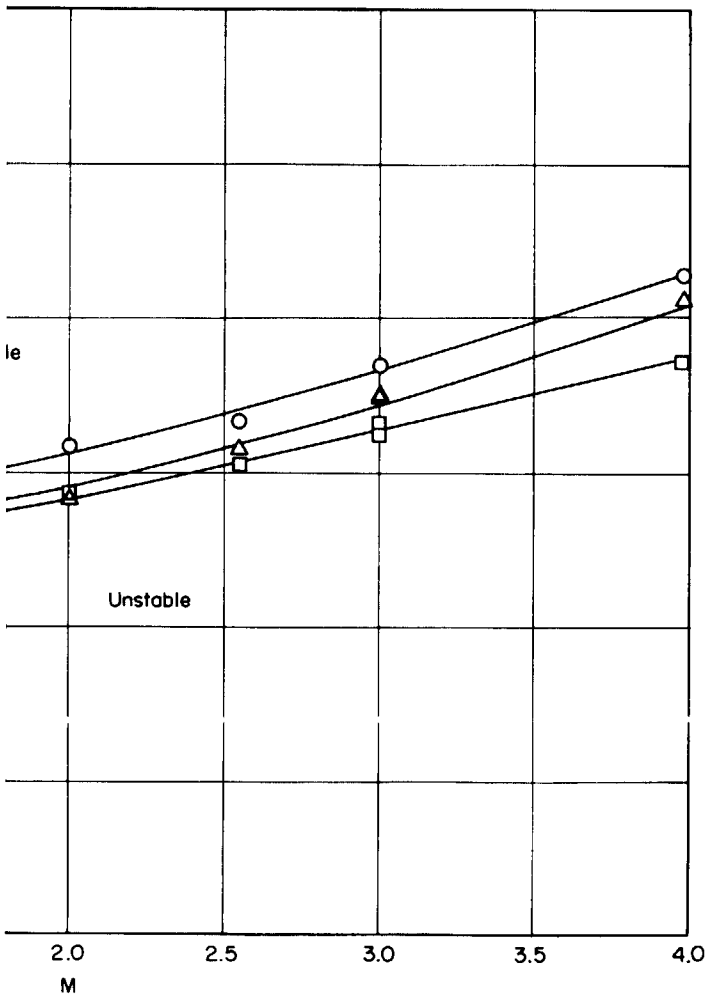

e-wedge airfoil.

2.- Concluded.

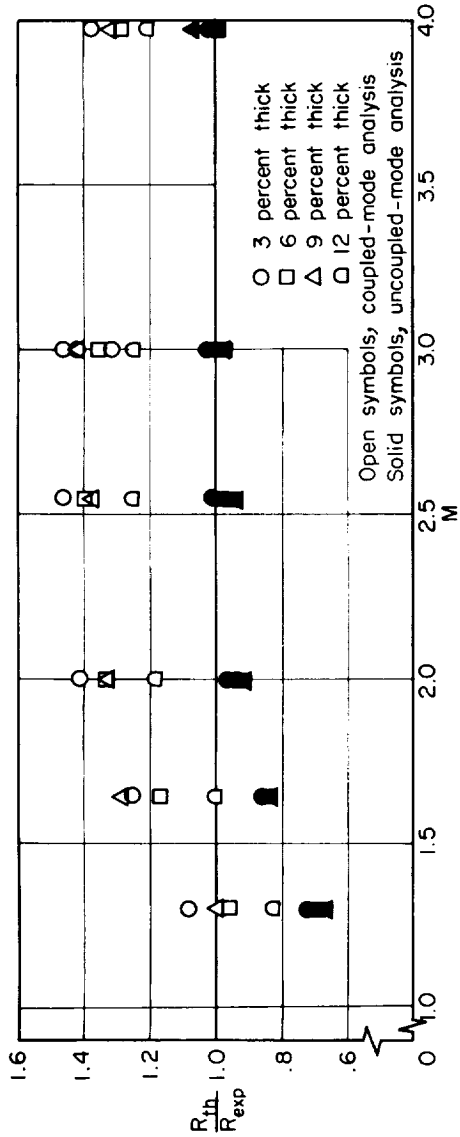

(a) Double-wedge airfoils.

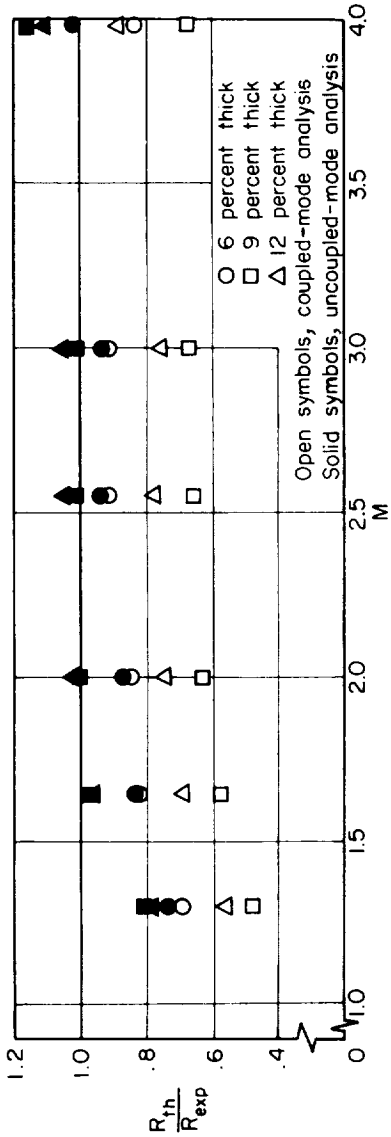

(b) Single-wedge airfoils.

Figure 14.- Comparison of experimental and calculated stiffness-altitude parameters for tapered models.

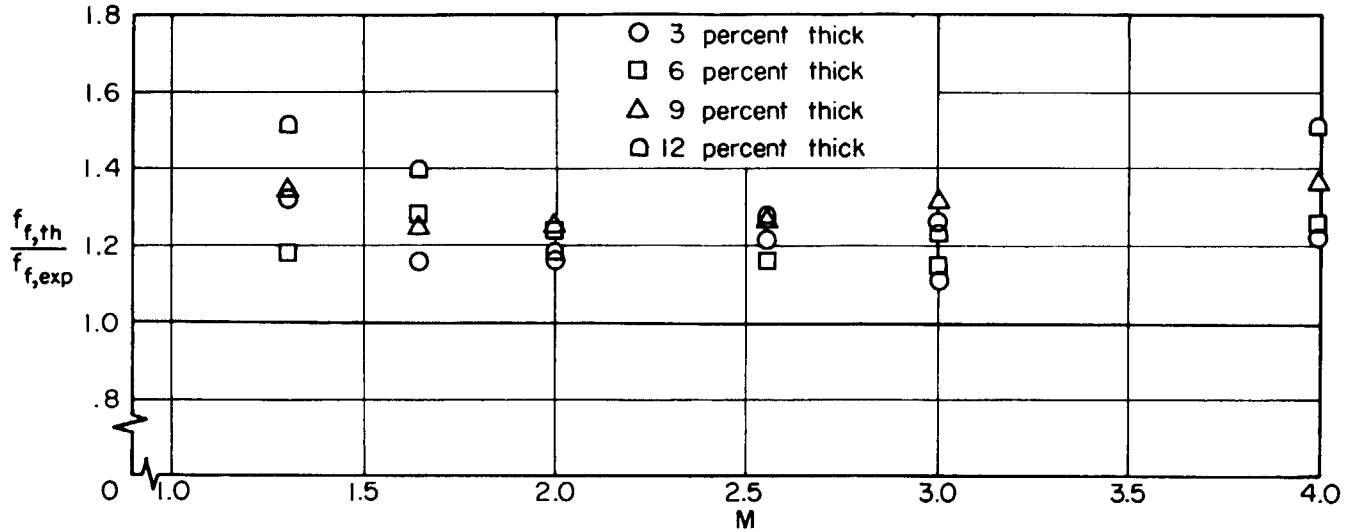

(a) Double-wedge airfoils; uncoupled-mode analysis.

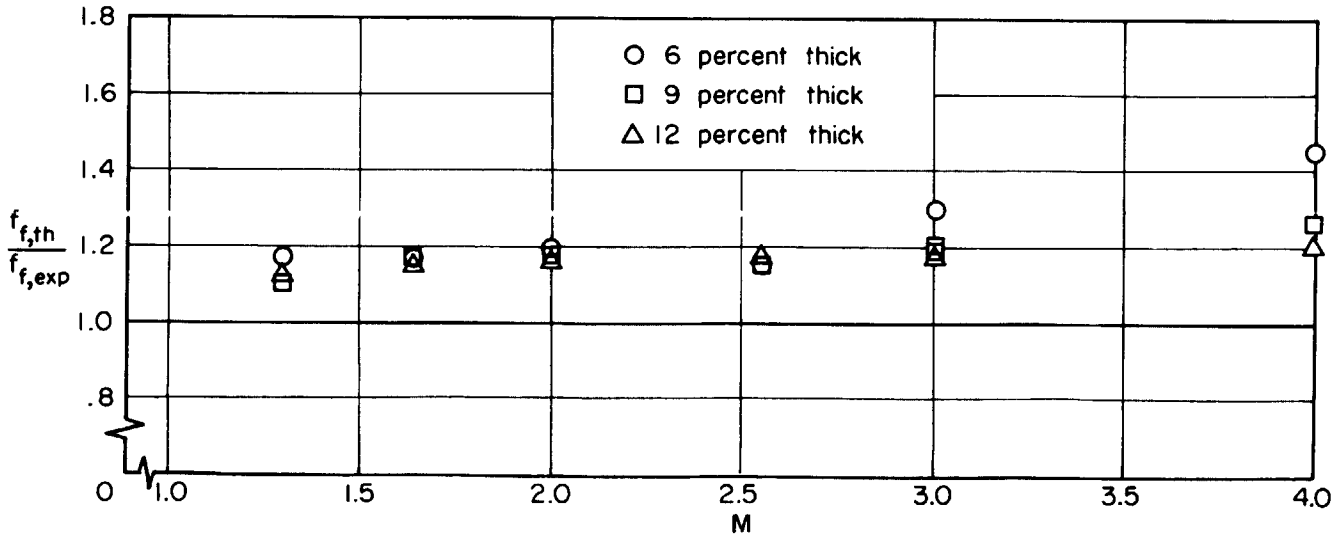

(b) Single-wedge airfoils; uncoupled-mode analysis.

Figure 15.- Comparison of experimental and calculated flutter frequencies for tapered models.

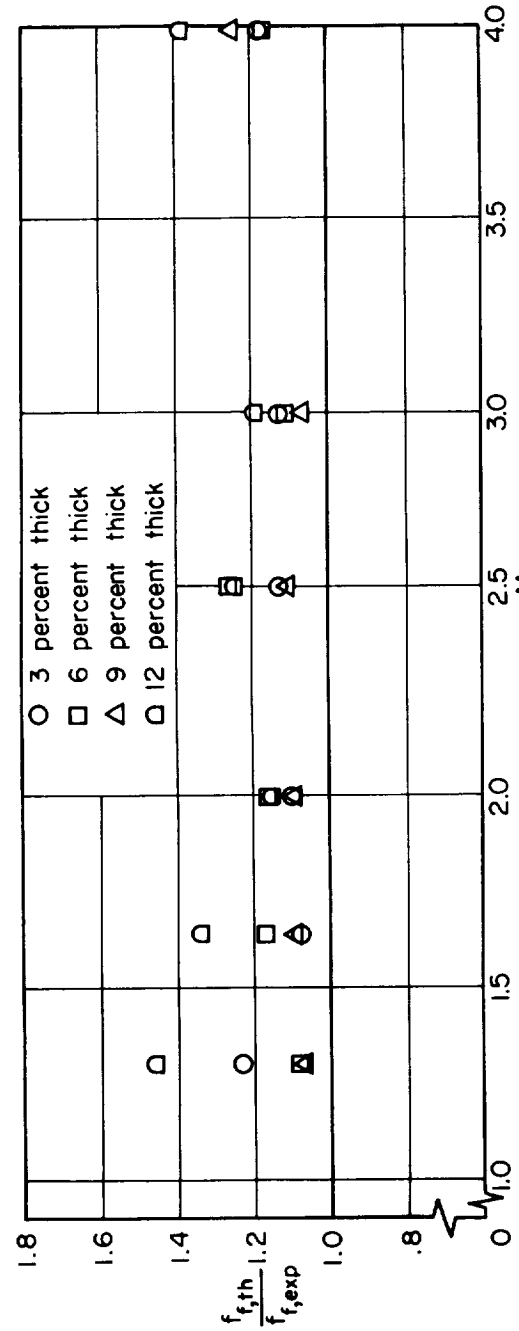

(c) Double-wedge airfoils; coupled-mode analysis.

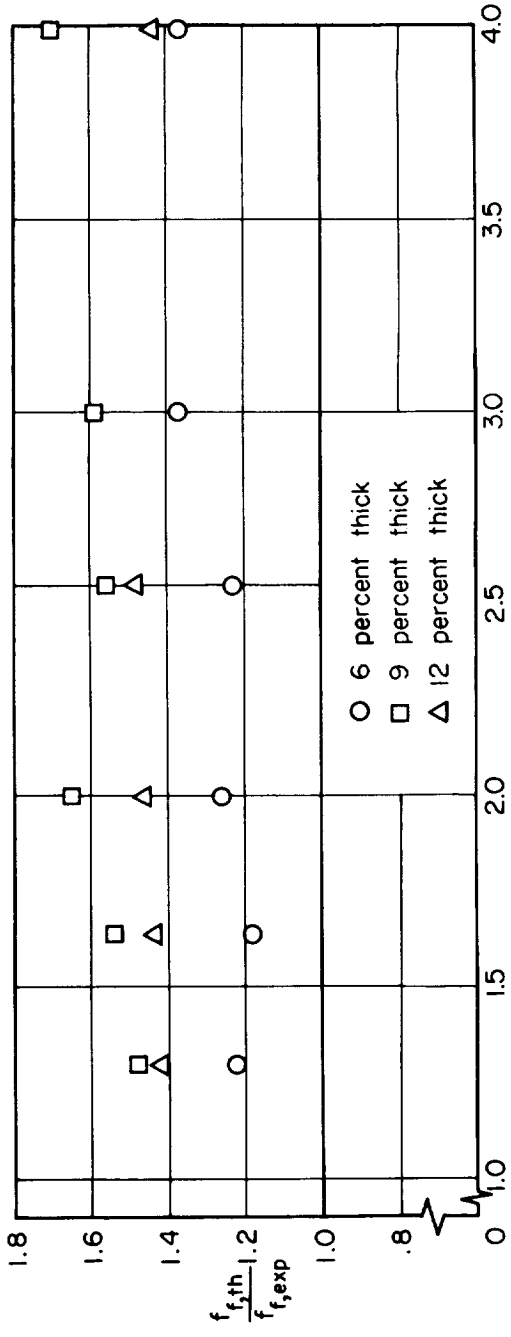

(d) Single-wedge airfoils; coupled-mode analysis.

Figure 15.- Concluded.